Bottom-up interactions in age-structured stock assessment and state-space mass-balance modelling

James T. Thorson[1], Kerim Y. Aydin[1], Matthew L. H. Cheng[2], Beatriz S. Dias[3], David G. Kimmel[4], Kasper Kristensen[5]

[1] Resource Ecology and Fisheries Management, Alaska Fisheries Science Center, National Marine Fisheries Service, NOAA

[2] Department of Fisheries at Lena Point, College of Fisheries and Ocean Sciences, University of Alaska Fairbanks, Juneau, Alaska 99801, USA

[3] Cooperative Institute for Climate, Ocean, and Ecosystem Studies, University of Washington, Seattle, WA, USA

[4] Recruitment Process Program, Alaska Fisheries Science Center, NOAA, NMFS, Seattle, Seattle, WA, USA

[5] Technical University of Denmark, Lyngby, Denmark

* Corresponding author: James.Thorson@noaa.gov

Abstract

Age-structured stock assessment models are used worldwide to predict the likely impact of changing harvest on future fisheries yield. However, age-structured models ignore the impacts of predator consumption on prey survival (top-down impacts) and prey availability on predator growth (bottom-up impacts), whereas multispecies statistical catch-at-age models often incorporate top-down but not bottom-up impacts. Here, we address this gap by demonstrating a generic approach for including bottom-up interactions in an age-structured statistical model by linking individual growth to population-scale consumption. We specifically extend Ecostate, a recent model that adapts Ecopath/Ecosim dynamics to jointly estimate biological and fishery parameters as well as unexplained process errors. We first add age-structured dynamics for select species using stanzas, i.e., an age-range over which age-structured productivity and consumption match mass-balance constraints. We then incorporate likelihood components representing fit to age-composition and empirical weight-at-age data while also estimating residual variation in larval survival (recruitment deviations) and consumption (weight-at-age deviations). To demonstrate, we fit to abundance-index and age-composition data for two commercial species (Alaska pollock and sablefish) in the Gulf of Alaska, including mass-balance dynamics for its primary energetic supply, and not fitting weight-at-age data so that it can be used for out-of-sample evaluation of model performance. We show that the model can be viewed as a multispecies age-structured model (e.g., estimating adult mortality rates, survey catchability and selectivity, and biomass while tracking cohorts) and as a mass-balance ecosystem model (e.g., estimate trophic position and weight-at-age based on forage consumption). The predicted weight-at-age is weakly correlated with independent measurements for pollock and sablefish, but were improved when we incorporated forage biomass indices. We

conclude that bottom-up interactions can be added to age-structured stock assessment models, and can address new questions regarding forage availability on weight-at-age for use in stock assessments.

Keyworks: Multispecies model; Ecopath with Ecosim; mass balance; state-space model; bottom-up interactions; age-structured dynamics

Introduction

Interest in how food availability affect productivity for marine species (i.e., "bottom-up interactions") is growing for several reasons:

1. *Climate change*: Primary production is changing due to global temperature and nutrient supply (Boyce & Worm, 2015), and regional changes in primary production may impact ecosystem-level sustainable harvest (Atkinson et al., 2024; Chassot et al., 2010). Similarly, changes in regional temperature can affect predator-prey overlap, and subsequently drive changes in consumption and species interactions (Goodman et al., 2022; Thorson et al., 2021);
2. *Managing harvest for forage species*: Alternatively, direct harvest of forage species such as Atlantic menhaden (Chagaris et al., 2020) and Antarctic krill (Trathan et al., 2022) have led managers to regulate harvest of forage species based on their impact on other fished or protected species;
3. *Changing size*: Changes in animal size are well documented and have large impacts on sustainability and human benefits for Pacific salmon (Oke et al., 2020) and for numerous groundfishes (Thorson et al., 2015). In well-documented examples such as Baltic cod, a change in forage abundance and consumption can then lead to decreased size-at-age for a commercially important fish (Neuenfeldt et al., 2020).

Given these varied motivations, there is a need for analytical methods that can identify "bottom-up" interactions in marine ecosystems.

Ecological models are often used to analyze the physical and ecological drivers for marine ecosystem changes. For example, age-structured stock-assessment models (ASSAM) are typically fitted to survey and fishery data and then used to predict the likely impact of alternative

fishery regulation on future biomass and harvest (Methot, 2009). Alternatively, multispecies statistical catch-at-age models (MSSCA) extend ASSAM by estimating biomass for multiple species, and then incorporate "top-down" drivers by predicting variation in natural mortality for a prey species based on the consumption by their predators (Begley & Howell, 2004; Jurado-Molina et al., 2005). More recently, there is increased research regarding state-space versions of MSSCA and ASSAM, which incorporate both variation in measurements ("measurement error") and variation in demographic rates over time ("process errors"). For example, state-space ASSAM have been developed that estimate changes in weight-at-age (Correa et al., 2023), and state-space MSSCA can estimate process errors in recruitment for individual species (Adams et al., 2022). These models (whether conventional or state-space) are typically fitted directly to data and then updated as needed to repeatedly inform management for a given stock or management question.

Despite their widespread use, ASSAM and MSSCA typically do not estimate "bottom-up" drivers, i.e., how prey biomass and resulting consumption subsequently affects the productivity (i.e., growth, reproduction, or survival) of their predators (although see Fitzpatrick et al., 2022). Instead, bottom-up drivers are typically analyzed using mass-balance or "end-to-end" ecosystem models that are generally not fitted directly to time-series data. For example, the mass-balance model Ecopath is typically balanced by estimating an unknown "ecotrophic efficiency" (the fraction of mortality rates attributed to modeled predators) given specified values for production and consumption per biomass as well as biomass and diet proportions for a list of interacting species (Polovina, 1984). Ecopath can then be projected over time using Ecosim (Walters et al., 1997), and Ecosim can incorporate age-structured dynamics (Walters et al., 2000) which then have important consequences for species interactions (Walters & Kitchell, 2001). Predator

functional-response parameters are sometimes estimated via fit to time-series data without otherwise fitting parameters in the original Ecopath mass-balance (Bentley et al., 2024; Scott et al., 2016). More recently, Ecostate was developed as a state-space extension to mass-balanced dynamics, and it estimated both bottom-up and top-down drivers for ecosystem dynamics in the eastern Bering Sea (Thorson et al., 2024). However, Ecostate was restricted to modelling biomass dynamics without age-structure, and therefore did not fit age-composition data, track cohort strength, estimate fishery selectivity, or incorporate other features that are common in ASSAM.

In this paper, we discuss how to incorporate bottom-up interactions into statistical age-structured models by linking individual growth to population-level consumption, and demonstrate the approach by extending Ecostate to include age-structured dynamics. We first outline how simple metabolic assumptions can link individual size-at-age to population-level consumption. We then summarize Ecostate and outline how it predicts weight-at-age from theory (biomass dynamics) and/or observations (biomass indices) for forage species. We then demonstrate the model by fitting to two age-structured populations (sablefish *Anoplopoma fimbria* and walleye pollock *Gadus chalcogrammus*) as well as their major forage pathways (pelagic production and benthic detritus via copepods and euphausiids) in the Gulf of Alaska. We evaluate model performance by (1) withholding real-world measurements of weight-at-age, and comparing these with model predictions of weight-at-age; (2) withholding and then forecasting later biomass index and age-composition data in a retrospective skill-testing experiment; and (3) evaluating how model performance changes when withholding survey indices for zooplankton forage. Our analysis demonstrates that state-space mass-balance models

serve as a useful middle-ground between stock and ecosystem modelling, and can attribute predator growth to their consumption of prey.

Methods

We seek to add bottom-up interactions to age-structured models by linking individual growth to population consumption. In the following, we adapt an approach derived from Ecopath with Ecosim (Lucey et al., 2020; Walters et al., 1997) and in particular Ecosim's multistanza extension (Walters et al., 2000) that can be repurposed in state-space mass balance and age-structured assessment models. The method requires:

1. Weight-at-age represented using the generalized von Bertalanffy function in a selected ("reference") time;
2. Consumption and metabolic demand that results in weight-at-age in that reference time;
3. Consumption and metabolic demand during a given time-interval, used to calculate growth in that interval relative to the reference time.

In the following, we define reference weight-at-age, consumption, and metabolic demand as values that occur in a model equilibrium (see Table S1 for a list of notation). However, future studies could apply the method to models without a defined equilibrium, and instead define growth relative to some initial consumption and weight-at-age. We proceed by first reviewing the theory from which this method is derived.

Individual growth and population consumption

Fish grow based on the balance between energetic supply (anabolism) and expenditure (catabolism), and von Bertalanffy (1969 Eq. 7.8) formalized this by theorizing that an animal with body size ω (in units mass) has growth rate $\frac{\mathrm{d}}{\mathrm{d}t}\omega$ that follows a differential equation[1]:

$$\frac{\mathrm{d}}{\mathrm{d}t}\omega = \underbrace{H\omega^{d}}_{\text{Anabolism}} - \underbrace{K\omega}_{\text{Catabolism}} \tag{1}$$

where d is the allometric increase in consumption with body size, H is the consumption per effective size, and K is the linear increase in catabolism with body mass (Essington et al., 2001). Integrating this expression over time where individuals start at zero mass (i.e., $\omega(0) = 0$) then results in the generalized von Bertalanffy growth function:

$$\omega(a) = \omega_{\infty}\left(1 - e^{K(1-d)a}\right)^{\frac{1}{1-d}} \tag{2}$$

where asymptotic weight $\omega_{\infty} = \left(\frac{H}{K}\right)^{\frac{1}{1-d}}$. When assuming that body mass scales isometrically (i.e., $\omega = aL^{b}$ where $b = 3$) and that consumption increases with length-squared (i.e., $d = \frac{2}{3}$), this expression reduces to the widely used von Bertalanffy model for length-at-age $L(a) = L_{\infty}(1 - e^{-ka})$ where $k = 3K$.

Although the von Bertalanffy length-at-age function is widely used in age-structured stock-assessment models, there are relatively few models that incorporate bottom-up interactions by linking individual growth rate $\frac{\mathrm{d}}{\mathrm{d}t}\omega$ (or growth increments using a linear approximation to $\frac{\mathrm{d}}{\mathrm{d}t}\omega$) to consumption. To make this link, let us first assume that a population has equilibrium weight-at-age $\bar{\omega}_a$ that arises from the generalized von Bertalanffy growth function (Eq. 2). It also has

[1] In the following, we use vector-matrix notation (see Edwards & Auger-Méthé, 2019), but introduce binary subscripts $s2$, $g2$, etc., due to running out of Roman letters for data and subscripts.

equilibrium age-distribution $\bar{\nu}_a$, and we define biomass $\beta = \sum_{a=0}^{a_{\max}} \nu_a \omega_a$ such that equilibrium biomass $\bar{\beta} = \sum_{a=0}^{a_{\max}} \bar{\nu}_a \bar{\omega}_a$.

We start by applying an Euler (piecewise linear) approximation to the von Betalanffy differential equation (Eq. 1) for equilibrium weight at age, while discretizing integer age a into n_Δ intervals, where fractional age $a^* = n_\Delta a + \Delta$ corresponds to interval Δ of integer age a:

$$\bar{\omega}_{a^*+1} = \bar{\omega}_{a^*} + \frac{H \bar{\omega}^d{}_{a^*}}{n_\Delta} - \frac{K \bar{\omega}_{a^*}}{n_\Delta} \tag{3}$$

We then assume that anabolism $\frac{H \omega_{a^*}^d}{n_\Delta}$ will vary with consumption, i.e.:

1. if there is no consumption, then anabolism $\frac{H \omega_{a^*}^d}{n_\Delta}$ is also zero and individuals are predicted to shrink at rate $\frac{\mathrm{d}}{\mathrm{d}t}\omega = -K\omega$ with linear approximation $\omega_{a^*+1} = \omega_{a^*} - \frac{K \omega_{a^*}}{n_\Delta}$
2. if consumption, weight-at-age, and abundance-at-age are all at their equilibrium, then we expect growth to also match its equilibrium value, and this occurs when anabolism is $\frac{H \bar{\omega}_{a^*}^d}{n_\Delta}$;
3. If consumption doubles relative to its equilibrium, we expect anabolism to also double.

As further complication, a model might track consumption Q only when aggregating across fractional ages. In the following, we partition fractional ages a^* into "stanzas" (a.k.a. stages) $s2$, and model equilibrium consumption $\bar{Q}_{s2}$ (or other quantities) by summing across fractional ages $a^* \in s2$ within a given stanza $s2$. Alternatively, a model might aggregate all fractional ages a^* into a stanza $s2$ representing a single integer age a, and track consumption Q_a for each integer age.

To proceed, we re-arrange the individual growth equation (Eq. 3) to show that anabolism at equilibrium for fractional age a^* is $\bar{\omega}_{a^*+1} - \bar{\omega}_{a^*} + \frac{K}{n_\Delta} \bar{\omega}_{a^*}$. Average individual anabolism must

be supported by population-scale consumption Q_{s2} for the corresponding stanza $s2$, and that stanza has metabolic demand $\sum_{a^{*\prime} \in s2} v_{a^{*\prime}} \omega_{a^{*\prime}}^{d}$. At equilibrium, we therefore have an identity:

$$\underbrace{\bar{\alpha}_{a^*} \left(\frac{\bar{Q}_{s2}}{\sum_{a^{*\prime} \in s2} v_{a^{*\prime}} \omega_{a^{*\prime}}^{d}} \right)}_{\substack{\text{Equilibrium consumption} \\ \text{per biomass for stanza } s2}} = \underbrace{\bar{\omega}_{a^*+1} - \bar{\omega}_{a^*} + \frac{K}{n_\Delta} \bar{\omega}_{a^*}}_{\substack{\text{Equilibrium anabolism for} \\ \text{fractional age a}^*}} \quad (4)$$

And solving for $\bar{\alpha}_{a^*} = \left(\bar{\omega}_{a^*+1} - \bar{\omega}_{a^*} + \frac{K}{n_\Delta} \bar{\omega}_{a^*} \right) \left(\bar{Q}_s / \sum_{a^* \in s2} \bar{v}_{a^*} \bar{\omega}_{a^*}^{d} \right)^{-1}$ then converts the ratio of consumption and metabolic demand for a given stanza $s2$ to anabolism for a given fractional age a^*. We can then use $\bar{\alpha}_{a^*}$ to calculate anabolism given other levels of consumption and metabolic demand:

$$\omega_{a^*+1} = \omega_{a^*} + \bar{\alpha}_{a^*} \frac{Q_{s2}}{\sum_{a^{*\prime} \in s2} v_{a^{*\prime}} \omega_{a^{*\prime}}^{d}} - \frac{K}{n_\Delta} \omega_{a^*} \quad (5)$$

This expression therefore links individual, age-specific growth increments to total consumption Q_2 aggregated over a set of ages fractional ages $a^* \in s2$. The expression satisfies our three objectives, i.e., (1) predicting a decline in size in the absence of consumption, with (2) weight-at-age matching equilibrium values given equilibrium age-structure and consumption, and also (3) having a linear increase in anabolism with consumption. Future research could modify the third characteristic by shunting elevated consumption into elevated survival or reproductive output (Walters et al., 2000), although we do not explore this here.

In the following, we demonstrate how Eq. 4-5 can be used to integrate bottom-up interactions into age-structured population dynamics. We specifically extend the state-space mass balance model Ecostate, which informs forage abundance based on both:

1. *Theory*, i.e., forage species follow a simple biomass-dynamics model such that they have some assumed or estimated density dependence where, e.g., predator growth will tend to increase as their fishing mortality rate increases (Fig. S1);

2. *Observations*, i.e., where forage biomass will closely match biomass indices when they are available, such that dynamics will condition upon observations (i.e. predicted growth will increase when forage indices increase).

In particular, we investigate whether having forage biomass indices can improve predictions of predator weight-at-age relative. However, future models could replace our density-dependent model for prey dynamics with user-specified indices of prey biomass or predator consumption (i.e., treating prey biomass or consumption as covariates).

State-space mass balance modelling

Ecostate (Thorson et al., 2024) is a state-space model for population-dynamics, which tracks biomass $\beta_s(t)$ for each $s \in \{1,2,\ldots,S\}$ of S functional groups in continuous time $t_{min} < t < t_{max}$. Functional groups are categorized as autotrophs (producers), heterotrophs (consumers), and detritus pools, and we index functional groups as prey i and predator j in expressions that involve predators and prey groups. It uses dynamical equations derived from Ecopath (Polovina, 1984) and Ecosim (Walters et al., 1997, 2000; Christensen & Walters, 2004) and extends these dynamics to permit: (1) any combination of parameters to be estimated via fit to time-series data using maximum likelihood, with options for likelihood penalties and/or Bayesian estimation; and (2) estimation of process errors representing unmodeled variation in dynamics, where the variance of process errors can be estimated as a hierarchical model. We first briefly summarize the previous development of Ecostate, before then introducing how age-structured models are incorporated.

Ecostate (mimicking Ecopath) first defines an equilibrium biomass $\bar{\beta}_s$, where biomass inputs (primary production, assimilated consumption, and detrital inputs) match outputs (metabolic

demand, biomass growth, natural mortality, predation mortality, and detrital turnover) on average for all functional groups. This equilibrium is expressed using the "master equation":

$$\underbrace{\bar{\beta}_i}_{\substack{\text{Equilibrium} \\ \text{biomass for prey i}}} \times \underbrace{p_i}_{\substack{\text{Prey} \\ \text{production} \\ \text{per biomass}}} \times \underbrace{e_i}_{\substack{\text{Prey} \\ \text{ecotrophic} \\ \text{efficiency}}} \tag{6}$$

$$= \sum_{j=1}^{S} \left(\underbrace{d_{i,j}}_{\substack{\text{Proportion of} \\ \text{diet for predator} \\ j \text{ by prey } i}} \times \underbrace{\bar{\beta}_j}_{\substack{\text{Equilibrium} \\ \text{biomass for} \\ \text{predator } j}} \times \underbrace{w_j}_{\substack{\text{Predator} \\ \text{consumption} \\ \text{per biomass}}} \right)$$

where p_i is production per biomass, e_i is the proportion of biomass that is utilized by modeled variables ("ecotrophic efficiency"), $d_{i,j}$ is diet proportions (where diet matrix **D** has columns that sum to one for heterotrophs and zero otherwise), and w_j is consumption per biomass. Fitting this equation requires that the analyst specify a fixed value (or estimate as fixed effect) three of the four parameters $\{p_s, e_s, \bar{\beta}_s, w_s\}$ for each taxon, and such that the fourth value can be solved deterministically (Polovina, 1984). We envision that analysts will typically solve for ecotrophic efficiency, although it could instead be estimated with a prior in cases when all predators are being modeled.

Ecostate (mimicking Ecosim) then defines a differential equation for biomass dynamics over time $\beta_s(t)$ given these same parameters:

$$\frac{d}{dt}\beta_s(t) = \left(\underbrace{g_s(t)}_{\substack{\text{Growth} \\ \text{rate}}} - \underbrace{m_s(t)}_{\substack{\text{Natural} \\ \text{mortality} \\ \text{rate}}} - \underbrace{f_s(t)}_{\substack{\text{Fishing} \\ \text{mortality} \\ \text{rate}}} + \underbrace{\epsilon_s(t)}_{\substack{\text{Process error} \\ \text{in biomass rate}}} \right) \beta_{s,t} \tag{7}$$

$$\frac{d}{dt}\eta_s(t) = f_s(t)\beta_s(t)$$

where $g_s(t)$ is a population growth rate, $m_s(t)$ is population mortality rate, $f_s(t)$ a fishing mortality rate, $\epsilon_s(t)$ is an optional process error in biomass rates, and $\eta_s(t)$ is an accumulator tracking fishery catches. Population growth $\mathbf{g}(t)$ and mortality $\mathbf{m}(t)$ are calculated based on a matrix of consumption rates, and see Table 1 for definitions. Biomass and catches across all groups are then integrated at an annual time-step by default $\left(\boldsymbol{\beta}(t+1), \boldsymbol{\eta}(t+1)\right) = \int_t^{t+1} \frac{d}{dt}\left(\boldsymbol{\beta}(t), \boldsymbol{\eta}(t)\right)$ numerically, e.g., using an Adams-Bashforth ordinary differential equation algorithm with user-specified accuracy (with other ODE solvers also available to users). The model can be fitted to a combination of biomass indices and fishery catch time-series (Thorson et al., 2024).

Combining age-structured and biomass dynamics

Here, we extend Ecostate to incorporate age-structured dynamics for selected heterotrophs. This extension starts using the "multistanzas" functionality from Ecosim (Walters et al., 2000), but incorporates new options to:

1. fit age-composition data, while weighting those data using a multinomial distribution with a known "input-sample size", or further down-weighting the input sample size using a Dirichlet-multinomial distribution as a diagnostic of model mis-specification (Thorson et al., 2023);
2. fit empirical weight-at-age data;
3. estimate logistic selectivity parameters via their fit to age-composition data;
4. estimate parameters representing equilibrium weight-at-age, i.e., von Bertalanffy growth rate, asymptotic weight, the allometric scaling of consumption to size, and the proportion of animals that are mature for each age ("maturation ogive");

5. estimate stock-recruit parameters representing equilibrium recruits and the steepness of the emergent stock-recruit relationship occurring at equilibrium conditions for other taxa;
6. estimate annual variation in cohort strength beyond what's expected from the stock-recruit relationship as a random effect ("recruitment deviations"), while potentially estimating the variance of recruitment-deviations using maximum marginal or penalized likelihood;
7. estimate annual variation in consumption for a given predator, beyond what's expected from the deterministic skeleton (Eq. T1.1).

These options have not previously been implemented in any model using Ecosim or extensions of the underlying equations. Collectively, these extensions allow us to use Ecostate to fit parameters for a full age-structured stock assessment model, including decadal projections, stock status, Bayesian priors, process errors, and model diagnostics. However, the age-structured model also incorporates both top-down (i.e., changes in natural mortality resulting from predator consumption) and bottom-up (i.e., changes in individual size resulting from consumption of prey) controls.

Following Ecosim, each age-structured population $g2$ is represented using one or more stanzas $s2[g2]$, and each stanza $s2$ is itself associated with a functional group $s[s2]$, such that the biomass for stanza-group of an age-structured population is $\beta_{s[s2[g2]]}$. To simplify presentation in the following, we discuss how age-structured dynamics are incorporated for a single population and suppress index $g2$ from notation throughout. However, the model (and associated code) is fully generic, and can incorporate age-structured dynamics for as many heterotrophs as specified by the user.

Stated briefly, Ecostate defines unfished equilibrium biomass $\frac{d}{dt}\bar{\beta}_s = 0$ for heterotroph s as occurring when the population growth $\bar{g}_s$ (which arises from consumption) balances population

mortality $\bar{m}_s$ (which arises from predation); mass balance for primary producers and detritus groups is detailed elsewhere (Thorson et al., 2024). To convert these biomass-dynamic rates to age-structured dynamics, Ecostate converts biomass mortality rate $m_s(t) + f_s(t)$ in Eq. 7 to an individual mortality rate (which has no direct effect on somatic growth rates) and converts biomass growth $\bar{g}_s(t)$ to an individual growth rate (which has no direct effect on individual mortality rates). Both conversions are specified to satisfy two conditions at unfished equilibrium:

1. the conversion of equilibrium population mortality $\bar{m}_s(t)$ to individual mortality rate results in a stable age-distribution. Given weight-at-age and the stable age-distribution, we can calculate biomass-per-recruit for a given stanza $s2$, and equilibrium recruitment is calculated as biomass $\beta_{s[s2]}$ divided by biomass-per-recruit for that stanza $s2$. We then use equilibrium recruitment, stable age-distribution, and weight-at-age to calculate biomass for other stanzas. Equivalently, this equilibrium occurs when production per biomass p_s for each stanza is equal to the mortality rate over the corresponding age-range and;
2. the conversion of equilibrium population growth rate $\bar{g}_s(t)$ to individual growth results in a generalized von Bertalanffy growth function with specified growth rate k, asymptotic weight W_∞, and allometric scaling d. This condition is met by solving for equilibrium consumption and consumptive demand, and then applying Eq. 4-5.

Further details are notation are provided in Supplementary Material 2.

Fitting to data

In particular, we calculate the likelihood of age-composition data $\mathbf{N}$ containing vector $\mathbf{n}_t$ of samples $n_{a,t}$ for each integer age a in year t. However, age-composition sampling typically

arises from a monitoring program with some selectivity-at-age s_a, so we estimate two parameters θ_1 and θ_2 that represent the logistic survey selectivity, $s_a = \left(1 + e^{\theta_1 - \frac{a}{\theta_2}}\right)^{-1}$:

$$\mathbf{n}_t \sim Multinomial\left(\frac{\mathbf{sv}(t)}{\sum_{a=1}^{a_{\max}} s_a v_a(t)}\right)$$

where $\sum_{a=1}^{a_{\max}} n_a(t)$ is the input sample size which determines the weighting of these data relative to other information. Alternatively, we can instead specify a Dirichlet-multinomial distribution:

$$\mathbf{n}_t \sim DM\left(\frac{\mathbf{sv}(t)}{\sum_{a=1}^{a_{\max}} s_a v_a(t)}, \theta_3\right)$$

Where θ_3 is (approximately) the ratio of input and effective sample size (Thorson et al., 2017).

Similarly, we calculate the likelihood of empirical weight-at-age data **W** containing the average body weight $w_{a,t}$ for each integer age and year. We specify a lognormal distribution:

$$\log\left(w_{a,t}\right) \sim Normal\left(\log\left(\omega_a(t)\right), \sigma_w^2\right)$$

where σ_w^2 is an estimated parameter representing the residual variance in weight-at-age data (and future research could incorporate sampling variability as an additional variance when fitting weight-at-age data). Model exploration suggests that age-composition data are informative about production-per-biomass p_{s2} (which is proportional to natural mortality rate), and that weight-at-age data are informative about the von Bertalanffy growth parameters k_{g2} and d_{g2}.

Finally, we also include options to estimate unexplained variation in age-structured dynamics:

1. *Recruitment deviations*: We estimate an annual "recruitment deviation" $\phi(t)$ which is assigned a normal distribution:

$$\phi(t) \sim Normal(0, \sigma_\phi^2)$$

where σ_{Φ}^2 is the variance of recruitment deviations, and can either be estimated using maximum marginal likelihood or fixed *a priori* when using penalized likelihood estimates. Recruitment deviations can then be informed by unexplained variation in age-composition data. Recruitment deviations will arise because cohort strength is strongly influenced by small differences in daily rates of larval survival resulting from ocean temperatures and advective fields (Cushing, 1990), which may be largely independent of trophic interactions represented within Ecostate.

2. *Consumption deviations*: Similarly, variation in oceanographic conditions (e.g., temperature) may drive variation in predator-prey overlap and/or predator metabolic demand. We therefore incorporate annual variation in predator consumption, where we replace the deterministic equation for consumption (Eq. T1.1) from Ecostate with a "semi-parametric" equation:

$$c_{i,j}(t) = \underbrace{\bar{c}_{i,j}}_{\substack{\text{equilibrium} \\ \text{consumption rate}}} \times \underbrace{\frac{x_{i,j}\frac{\beta_j(t)}{\bar{\beta}_j}}{x_{i,j} - 1 + \frac{\beta_j(t)}{\bar{\beta}_j}}}_{\substack{\text{predator functional} \\ \text{response}}} \times \underbrace{\frac{\beta_i(t)}{\bar{\beta}_i}}_{\substack{\text{prey functional} \\ \text{response}}} \times e^{\nu_j(t)}$$

where we again assign a normal distribution to consumption deviations:

$$\nu_j(t) \sim Normal(0, \sigma_{\nu,j}^2)$$

Where this variation can again be either estimated or fixed *a priori* depending upon computational constraints. An increase in consumption then decreases survival for prey species and also increases weight gain for the predator. Annual variation in consumption can therefore be informed either via unexplained variation in prey biomass, and/or predator weight-at-age.

3. *Survival deviations*: We note that process errors can be estimated for the biomass of any functional group, and this includes stanza of age-structured populations. Ecostate is parameterized such that process errors result in unexplained variation in survival rates when applied to age-structured groups. These process errors can then represent either excess mortality or immigration/emigration, similar to their interpretation in state-space age-structured models (Stock et al., 2021).

Parameter estimation

Building upon the mass-balance model Ecostate, we continue to estimate parameters using RTMB (Kristensen, 2024). This then provides a user-friendly interface to automatic differentiation (AD) and the Laplace approximation provided by TMB (Kristensen, 2014). However, age-structured calculations in Ecostate involve large matrices of abundance-at-age and weight-at-age for fractional ages a^* and years t^*. Given the size of the AD tape, it is not feasible to repeatedly calculate the Hessian matrix as required when using the Laplace approximation to apply maximum marginal likelihood. We therefore optimize the penalized likelihood while fixing the variance of random effects at values that are specified a priori. Future research could estimate these parameters via a hierarchical Bayesian model, i.e., using tmbstan (Monnahan & Kristensen, 2018) to sample the joint likelihood, but we do not explore the topic further here.

Case study demonstration

To demonstrate, we fit the model to age-structured survey data for two commercially important species (walleye pollock and sablefish) as well as their primary energetic pathways (i.e., zooplankton, benthic invertebrate fauna, primary producers, and benthic detritus) in the Gulf of Alaska. These data include:

1. Survey data for pollock from a stratified random bottom-trawl survey conducted biennially from 1990 to 2023 by the AFSC (Siple et al., 2024). Design-based estimators are used to generate a biomass index, age-composition (in numbers, excluding 2023), and average weight-at-age. Survey data east of 140W are excluded as there is evidence that is a separate stock. Total catches from 1970-2023 were also used, and details about how they were obtained can be found in Monnahan et al. (2023).
2. Survey data from a cooperative longline survey for sablefish, which follows a systematic survey design, including age-composition (in numbers), empirical weight-at-age, and a biomass index (in mass). We reprocessed the data to only include sets in the Gulf of Alaska, i.e. excluding stations occurring in the Bering Sea or Aleutian Islands. Given the unknown area of attraction for longline gear, the biomass index is calculated using a depth-stratified, area-weighted estimator, and the biomass time-series is treated as a relative index (i.e., estimating a catchability coefficient).
3. Total annual fishery harvest for the two directed fisheries, extracted from the most recent stock assessments for pollock (Monnahan et al., 2023) and sablefish (Goethel et al., 2024);
4. An Rpath model for the Western Gulf of Alaska, where we use annual biomass production per biomass p_s, annual consumption per biomass w_s (which includes digested and unassimilated consumption in biomass), and the diet proportions matrix $d_{i,j}$, as well as equilibrium biomass $\bar{\beta}_s$ for those species where Ecostate is unable to estimate this based on available information.
5. A biomass index for large copepods from the EcoFOCI survey; Large copepod (> 2mm; example species: *Calanus* spp. and *Neocalanus* spp.) abundance (numbers per cubic meter) was estimated from 505 μm mesh, 60 cm diameter bongo nets. Total large copepod

abundance is summed for each station sampled within a two core areas, one in spring and one in summer, and the mean abundance is calculated from all stations within the core areas (Kimmel et al., 2023).

6. A biomass index for euphausiids from the Seward Line (Hopcroft, 2023).

We note that the sablefish stock assessment includes data from the Gulf of Alaska, Bering Sea, and Aleutian Islands, and therefore does not exactly match our spatial scale (which is restricted to the Gulf of Alaska). Similarly, the pollock assessment uses a somewhat restricted spatial scale that excludes southeast Alaska. We instead use the spatial scale of the Rpath model for the Western Gulf of Alaska, and expect that the difference in spatial scale will results in some differences in model results relative to estimates from each stock assessment.

For each age-structured population, we estimate unfished biomass for juveniles and adults (four scale parameters; Table 2). We also estimate the catchability coefficient and two logistic selectivity parameters for the primary survey of each species. To match the pollock stock assessment, we specify a lognormal likelihood penalty on the bottom-trawl survey catchability for pollock, with log-mean of $\log(0.85)$ and log-standard deviation of 0.1. To match the two stock assessments, we also fix steepness $h = 0.999$ (i.e., approaching a constant stock-recruit relationship) and estimate recruitment deviations $\phi_s(t)$. For both sablefish and pollock, we assumed that input-sample size for age-composition data was 60 in each year, and used the Dirichlet-multinomial likelihood to weight these data. However, the effective sample size approached the input value (60) for both species, such that we then reverted to nominal weighting using the multinomial likelihood. We also fix age-at-maturity $a_{\mathrm{mat}} = 6$ for sablefish and $a_{\mathrm{mat}} = 4$ with logistic slope $w_{\mathrm{matslope}} = 1$ to (approximately) match the sablefish and pollock assessments, and fix juvenile natural mortality at values from the Rpath model ($M =$

399 1.65 and 1.96 for sablefish and pollock, respectively). We estimate adult natural mortality rate
400 for each age-structured species, while specifying a likelihood penalty centered on the value
401 assumed in the stock assessment (sablefish: 0.1; pollock: 0.30) and with a log-standard deviation
402 of 0.1. We specify specialized von Bertalanffy growth rate $k = 0.14$ for sablefish and $k = 0.2$
403 for pollock, and also allometric consumption $d = \frac{1}{2}$ for sablefish and $d = \frac{2}{3}$ for pollock. These
404 are fixed here (because we are withholding weight-at-age data for model evaluation), but model
405 exploration suggests that they are estimable when fitting to weight-at-age data.
406 To represent species interactions, we estimate a vulnerability parameter $x_{ij} = x_j$ representing
407 the constant vulnerability all prey i for each of sablefish or pollock as predators j (Table 2), and
408 specify a lognormal penalty on vulnerability x_j with log-mean $\log(2)$ and log-standard deviation
409 of 1.0 (where 2 is the default value used in most Ecosim implementations). In addition, we
410 estimate the catchability coefficient for large copepods and euphausiids (such that estimated
411 biomass will tend to match the assumed equilibrium biomass fixed from Rpath), and also
412 estimate process-errors $\epsilon_s(t)$ for biomass dynamics of copepods and euphausiids (to allow the
413 model to match observed cycles and trends for zooplankton forage). Given that we are using
414 penalized likelihood (to avoid the computational cost of computing the Laplace approximation),
415 we fix the variance of recruitment deviations (i.e., $\sigma_\phi^2 = 1^2$ for both case study species) and also
416 fix the variance of process errors for copepods and euphausiids (i.e., $\sigma_\epsilon^2 = 1^2$ for both).
417 However, we confirm that the average across years of the standard-error squared and the sample
418 variance for deviations approximately matches the input variance (i.e., the tuning metric
419 discussed in Methot and Taylor (2011)).
420 To evaluate model performance, we explore:

1. *Predictive performance for weight-at-age*: We do not fit weight-at-age data directly. Instead, we use the model to predict annual weight-at-age and then compare these predictions with out-of-sample weight-at-age measurements. We explore this comparison visually, but also calculate the Pearson correlation between log-prediction and log-measurement for each age separately and then average this correlation across ages;
2. *Retrospective skill*: We conduct a retrospective experiment where we exclude all biomass index and age-composition data after year T. However, we retain data for fishery catches in all years, such that forecasts condition upon fishery harvest that matches the real-world observations in forecast years. We then forecast dynamics for year $T+1$ through 2040. We fit 10 "retrospective peals" where the year of last data $T = \{2022, 2021, \ldots, 2013\}$, and record the forecast (and standard error) for biomass and recruitment-deviations ϵ_t for pollock and sablefish. We compare these forecasts and standard errors with the estimates arising when fitting to all data ($T = 2023$);
3. *Value of zooplankton biomass information*: We compare the base model with an alternative scenario where we exclude biomass indices for zooplankton forage (euphausiids and copepods). This also requires eliminating the catchability coefficient for these indices as well as process-error deviations for these taxa. We then visually examine how this changes estimates of biomass trends for all taxa, as well as its impact on the out-of-sample predictions for weight-at-age for sablefish and pollock.

We also evaluate predictive performance (#1 above) by comparing predicted weight-at-age against a smoothed version of measured weight-at-age, estimated using a state-space model that includes age, year, and cohort effects (Cheng et al., 2024). This state-space model is intended to

filter out measurement error in the observed weight-at-age (resulting from low but known sample sizes) prior to the comparison with predictions from Ecostate.

Collectively, the model estimates population scale for the two age-structured populations while tracking cohorts, and also predicts time-varying natural mortality (from cannibalism and predation) and growth (from consumption and weight-specific metabolism). We can therefore view the model from two perspectives: as a stock-assessment model with two age-structured populations, and as a mass-balance model with species interactions. We therefore organize the Results to highlight these two perspectives.

Results

Stock assessment model with age-structured dynamics

Inspecting model output from a stock-assessment perspective, we see clear evidence in the age-composition for sablefish (Fig. 1) of a strong cohort born in 1997 (showing up at age-4 in 2001), 2005 (showing up at age-5 in 2009), and again in 2014 and 2016 (showing up at age-3 in 2017 and 2019). As expected, these cohorts result in increasing biomass as they grow through the population, i.e., from 2001-2003, 2008-2010, and again from 2017-2023 (Fig. 2). These latter cohorts result in adult sablefish biomass in 2023 approaching a high last seen at the beginning of biomass-index data (1990). However, biomass relative to equilibrium unfished is still expected to increase over subsequent years towards the unfished equilibrium (Fig. S2) under the scenario projected here (i.e. no catches after 2023).

Similarly, inspecting survey age-composition for walleye pollock (Fig. 3), we see strong cohorts in 1988 (showing up at age-2 in 1990 and age-5 in 1993), 2000 (ages 1/3/5/7 in 2001 onward), 2004 (ages 1/3/5 starting in 2005), and 2012 (showing up at ages 1/3/5). Finally, there is preliminary information about important cohorts in 2016 and 2020, which show up at ages-1

and later despite the continuing size of the 2012 cohort. The 2000 cohort is associated with rapid increases in adult biomass from 2001-2003, and the 2004 cohort causes an increase from 2006-2009 (Fig. 3). Finally, the strong recent cohorts have driven an increase from 300 to over 1000 kilotons from 2020-2023. Under a scenario of no future fishing, pollock biomass is then expected to decline slightly towards its unfished equilibrium (Fig. S2).

Mass-balance model with species interactions

Inspecting model output from a mass-balance model perspective (Fig. 4), we see that adult sablefish has a trophic level (TL) of 4.1 due to consuming adult pollock (TL: 3.6), while juveniles of both species have similar trophic position (TL: 3.6; see Table 2). As expected given this higher TL, adult sablefish has a lower natural mortality rate (0.10) than adult pollock (0.41) and also has a lower total biomass (adult sablefish: 361 kilotons; adult pollock: 1,609 kilotons).

The model estimates process errors in biomass dynamics for euphausiids and large copepods, which result in estimated biomass that closely matches available biomass-index data (Fig. 2). It then predicts interannual variation in zooplankton consumption and resulting weight-at-age for pollock and sablefish (Fig. 5 top row). Euphausiids are predicted to have cyclic variation in biomass with highs in 2002, 2009, and 2018, with both highs and lows generally decreasing over that period. By contrast, large copepods are predicted to decline consistently from 2005-2015 before subsequently stabilizing (Fig. 2).

Skill assessment #1: Out-of-sample weight-at-age predictions

Adult pollock weight-at-age is predicted to increase from 1993-2002 and then decline from 2002-2015 (Fig. 5 top-right panel). This increase and subsequent decrease in adult pollock weight-at-age is attributed to the increase and subsequent decline in euphausiid abundance, associated pollock consumption, and resulting weight-at-age (Fig. S3). Following 2016, adult

pollock are then predicted to have increasing weight-at-age, associated with an increase in adult pollock cannibalism resulting from the strong 2011 cohort (Fig. S3 bottom-right panel). These predicted patterns in weight-at-age are moderately (0.31) correlated with held-out survey measurements of weight-at-age, which also show a progressive increase from 1993-2002 but also a later peak in 2008-2012, and no evidence of an increase in 2018 onward (Fig. 5 bottom-right panel).

Similarly, the model predicts a peak in adult sablefish weight-at-age in 2014 (when adult sablefish is approaching its lowest levels), and a subsequent drop below equilibrium weight-at-age (Fig. 5 top-left panel). These predictions have a weakly negative (-0.13) correlation with held-out measurements of weight-at-age, which show declines for ages 2-10 and increases for the oldest ages (Fig. 5 bottom-left panel). The correlation between predictions and out-of-sample data is largely unchanged for pollock when comparing against smoothed measurements, but is somewhat more negative for sablefish (Fig. S4)

Skill assessment #2: Retrospective skill testing

Finally, we conduct a retrospective experiment removing data, forecasting dynamics under future catches, and comparing forecasts with subsequent predictions when fitting all data (Fig. 6). The model has information to precisely estimate recruitment deviations $\phi(t)$ for sablefish three to four years after a given year-class (e.g., the 2019 year-class has stabilized using data through 2022 or 2023), whereas for pollock it estimates them two to three years after (e.g., the 2019 year-class has stabilized by 2021) and there is preliminary evidence in 2023 data of a strong year-class in 2021.

These retrospective estimates of year-class strength then propagate forward during biomass forecasts. Forecasted biomass is generally within the 95% confidence interval even

when removing 10-years of data, although 10-year forecasts of adult pollock biomass range from essentially zero to twice the unfished equilibrium value (Fig. 6 1st and 2nd rows). Sablefish biomass has increased faster from 2020 onward than what was expected using data available in 2020 (which did not have information about higher-than-average recruitment after 2016, Fig. 6 3rd row). Similarly, adult pollock biomass forecasts have very broad confidence intervals when forecasting 6+ years forward, and recent biomass in 2020-2023 is lower than expected in 2013-2015 (Fig. 6 2nd row) due to lower-than-average recruitment from 2013-2020 (Fig. 6 4th row).

Skill assessment #3: Value of zooplankton indices

When we remove indices for copepods and euphausiids, predicted euphausiid biomass then has a strong negative correlated with adult pollock biomass and copepods have a strong positive correlation (Fig. S5), which contrasts strongly with the model predictions when fitting indices for these zooplankton species (Fig. 2). Predicted patterns in weight-at-age for sablefish and pollock are then different due to changes in predicted consumption of large copepods and euphausiids, and the correlations between predicted and observed weight-at-age declines for both fishes (Fig. S6).

Discussion

In this paper, we summarized a generic method to incorporate bottom-up interactions in age-structured population models, which calculates individual growth rates from population-level consumption relative to metabolic demand. This method uses a minimum of additional information, i.e., weight-at-age and consumption in a reference time and variable consumption used to calculate growth increments during other times. It could therefore be repurposed in other models as long as prey forage and/or consumption is modeled or specified as covariate. We then integrate the method into a recent state-space mass balance model Ecostate, and used modern

statistical computing (e.g., automatic differentiation) to efficiently estimate both demographic rates (e.g., equilibrium recruitment), measurement parameters (e.g., catchability coefficients and survey selectivity-at-age), and process errors (e.g., recruitment deviations) using penalized likelihood estimation. This represents the first (to our knowledge) effort to combine state-space age-structured modelling with multispecies modelling that includes both top-down and bottom-up interactions, and the resulting model can be viewed as both a stock-assessment and a mass-balance ecosystem analysis.

Many hypothesized mechanisms linking climate to fish productivity are mediated by forage availability, e.g., where increased temperature may impact productivity either positively (increase individual growth) or negatively (drive starvation mortality) depending on whether fish can compensate via increased consumption. In our case study, we showed that Ecostate can fit abundance-index and age-composition data for multiple age-structured species, and that fitting to forage biomass indices improves out-of-sample predictions of predator weight-at-age. We therefore recommend future research that attributes historical variation in weight-at-age to climate-linked variation in forage species. For species where these links can be identified, we then envision seasonal-to-decadal forecasts and multidecadal projections of predator weight-at-age as a potential next step. We therefore envision that future research is needed to understand how additional mechanisms (e.g., prey switching and temperature-dependent metabolism) drive weight-at-age in these species. This would extend recent research that attempts to link weight-at-age directly to ocean physics without considering forage availability or consumption (Oke et al., 2022).

Our analysis links individual consumption to population-scale consumption by adapting a differential equation for growth based on anabolism and catabolism (Eq. 1). However, Von

Bertalanffy (1960) additionally hypothesized that (1) both anabolism rate H and catabolism rate K would increase with temperature, and (2) anabolism would increase with temperature faster than catabolism. This second assumption then predicts that increased temperature leads to faster juvenile growth and slower adult growth (Morita et al., 2010), which has sometimes been called the "temperature-size rule" (Oke et al., 2022). Although debates continue about whether this pattern is widely observed (Atkinson, 1994), von Bertalanffy's first hypothesis is widely supported (Kingsolver & Huey, 2008). We therefore also recommend future research to incorporate a temperature-dependent link in both anabolism and catabolism parameters (H and K in Eq. 1). This would then allow future studies to investigate the impact of ocean temperature on fish productivity via both forage availability (population-level consumption) as well as bioenergetics (individual-level metabolism and foraging rates.

Despite these ecological and management reasons to study bottom-up drivers for weight-at-age, we also note several drawbacks in the implementation involving Ecostate. Most significantly, fishery mortality must be assigned a priori to a given stanza, and therefore fishery selectivity cannot be estimated using an age- or length-based function as is common in age-structured models. Future research could relax this assumption, although it would require some restructuring in how age-structured fishing mortality (Eq. 6) is represented when integrating biomass-dynamics for all functional groups (Eq. 2). We also have not represented demographic differences in sexually dimorphic species (e.g., sablefish). Future research could approximate this by modelling males and females as separate age-structured populations, although this would require pre-processing data to separately model the two. We also have not added detailed indexing for multiple survey and fishery fleets to the software package Ecostate, although this does not pose any fundamental difficulties beyond a more-complex user interface. Finally, we

have not incorporated any functionality to fit length-composition data. This would presumably require further research to identify how changes in consumption affect skeletal growth (length-at-age) relative to morphometric condition (weight-at-length), and how best to parameterize this tradeoff (e.g., Correa et al., 2023).

We also encourage further research to fit directly to consumption data resulting from stomach-content and diet samples. Stomach-content data can be standardized to estimate annual variation in both consumption and diet. We envision that these data could by fitted either as an index of total consumption and compositional data regarding diet proportions, or alternatively as a set of indices of prey-specific consumption. These two alternative options are somewhat analogous to the split between fitting age-based survey data as an abundance index and age-compositions, or as a matrix of abundance-at-age, and there are benefits and drawbacks to both approaches (Thorson et al., 2023). Regardless of which parameterization is used, we envision that stomach-content data could be used to identify prey-switching, temperature-dependent changes in consumption, and other realistic complications that arise in trophic ecology. We hope that (1) greater flexibility in representing predator consumption combined with (2) diet and consumption data from stomach contents will then allow future studies to better match observed variation in predator weight-at-age.

Acknowledgements

We are heavily indebted to the Rpath development team and Lucey et al. (2020), which previously described many of the Ecopath and Ecosim equations. We also thank M. Haltuch, D. Goethel, and A. Whitehouse for previous suggestions and discussions, C. Monnahan for providing stock-assessment inputs for Alaska pollock, R. Hopcroft for previously providing the

euphausiid biomass time-series, and A. Whitehouse and G. Adams for helpful comments on a previous draft.

References

Adams, G. D., Holsman, K. K., Barbeaux, S. J., Dorn, M. W., Ianelli, J. N., Spies, I., Stewart, I. J., & Punt, A. E. (2022). An ensemble approach to understand predation mortality for groundfish in the Gulf of Alaska. *Fisheries Research*, *251*, 106303. https://doi.org/10.1016/j.fishres.2022.106303

Atkinson, D. (1994). Temperature and Organism Size—A Biological Law for Ectotherms? In M. Begon & A. H. Fitter (Eds.), *Advances in Ecological Research* (Vol. 25, pp. 1–58). Academic Press. https://doi.org/10.1016/S0065-2504(08)60212-3

Atkinson, Rossberg, A. G., Gaedke, U., Sprules, G., Heneghan, R. F., Batziakas, S., Grigoratou, M., Fileman, E., Schmidt, K., & Frangoulis, C. (2024). Steeper size spectra with decreasing phytoplankton biomass indicate strong trophic amplification and future fish declines. *Nature Communications*, *15*(1), 381. https://doi.org/10.1038/s41467-023-44406-5

Begley, J., & Howell, D. (2004). *An overview of Gadget, the globally applicable area-disaggregated general ecosystem toolbox*. https://imr.brage.unit.no/imr-xmlui/bitstream/handle/11250/100625/FF1304.pdf?sequence=1

Bentley, J. W., Chagaris, D., Coll, M., Heymans, J. J., Serpetti, N., Walters, C. J., & Christensen, V. (2024). Calibrating ecosystem models to support ecosystem-based management of marine systems. *ICES Journal of Marine Science*, *81*(2), 260–275. https://doi.org/10.1093/icesjms/fsad213

Bertalanffy, L. V. (1969). *General System Theory: Foundations, Development, Applications* (Revised edition). George Braziller Inc.

Boyce, D. G., & Worm, B. (2015). Patterns and ecological implications of historical marine phytoplankton change. *Marine Ecology Progress Series*, *534*, 251–272. https://doi.org/10.3354/meps11411

Chagaris, D., Drew, K., Schueller, A., Cieri, M., Brito, J., & Buchheister, A. (2020). Ecological Reference Points for Atlantic Menhaden Established Using an Ecosystem Model of Intermediate Complexity. *Frontiers in Marine Science*, *7*. https://doi.org/10.3389/fmars.2020.606417

Chassot, E., Bonhommeau, S., Dulvy, N. K., Mélin, F., Watson, R., Gascuel, D., & Le Pape, O. (2010). Global marine primary production constrains fisheries catches. *Ecology Letters*, *13*(4), 495–505. https://doi.org/10.1111/j.1461-0248.2010.01443.x

Cheng, M., Goethel, D. R., Hulson, P.-J. F., Echave, K. B., & Cunningham, C. J. (2024). 'Slim pickings?': Extreme large recruitment events may induce density-dependent reductions in growth for Alaska sablefish (Anoplopoma fimbria) with implications for stock assessment. *Canadian Journal of Fisheries and Aquatic Sciences*, cjfas-2024-0228. https://doi.org/10.1139/cjfas-2024-0228

Christensen, V., & Walters, C. J. (2004). Ecopath with Ecosim: Methods, capabilities and limitations. *Ecological Modelling*, *172*(2), 109–139. https://doi.org/10.1016/j.ecolmodel.2003.09.003

Correa, G. M., Monnahan, C. C., Sullivan, J. Y., Thorson, J. T., & Punt, A. E. (2023). Modelling time-varying growth in state-space stock assessments. *ICES Journal of Marine Science*, *80*(7), 2036–2049. https://doi.org/10.1093/icesjms/fsad133

Cushing, D. H. (1990). Plankton production and year-class strength in fish populations: An update of the match/mismatch hypothesis. *Advances in Marine Biology*, *26*, 249–293.

Edwards, A. M., & Auger-Méthé, M. (2019). Some guidance on using mathematical notation in ecology. *Methods in Ecology and Evolution*, *10*(1), 92–99. https://doi.org/10.1111/2041-210X.13105

Essington, T. E., Kitchell, J. F., & Walters, C. J. (2001). The von Bertalanffy growth function, bioenergetics, and the consumption rates of fish. *Canadian Journal of Fisheries and Aquatic Sciences*, *58*(11), 2129–2138.

Fitzpatrick, K. B., Weidel, B. C., Connerton, M. J., Lantry, J. R., Holden, J. P., Yuille, M. J., Lantry, B., LaPan, S. R., Rudstam, L. G., Sullivan, P. J., Brenden, T. O., & Sethi, S. A. (2022). Balancing prey availability and predator consumption: A multispecies stock assessment for Lake Ontario. *Canadian Journal of Fisheries and Aquatic Sciences*, *79*(9), 1529–1545. https://doi.org/10.1139/cjfas-2021-0126

Goethel, D. R., Hanselman, D. H., Rodgveller, C. J., Fenske, K. H., Shotwell, S. K., Echave, K. B., Malecha, P. W., Siwicke, K. A., & Lunsford, C. R. (2024). *Assessment of the sablefish stock in Alaska*. https://www.researchgate.net/profile/Matthew-Cheng-15/publication/370978839_2022_Alaska_Sablefish_Stock_Assessment_and_Fishery_Evaluation_SAFE_Report/links/646d2cb937d6625c002c5dae/2022-Alaska-Sablefish-Stock-Assessment-and-Fishery-Evaluation-SAFE-Report.pdf

Goodman, M. C., Carroll, G., Brodie, S., Grüss, A., Thorson, J. T., Kotwicki, S., Holsman, K., Selden, R. L., Hazen, E. L., & De Leo, G. A. (2022). Shifting fish distributions impact predation intensity in a sub-Arctic ecosystem. *Ecography*, *2022*(9), e06084. https://doi.org/10.1111/ecog.06084

671 Hopcroft, R. R. (2023). Spring and Fall Large Copepod and Euphausiid Biomass: Seward Line.
672 In B. Ferriss (Ed.), *Ecosystem Status Report 2023: Gulf of Alaska, Stock Assessment and*
673 *Fishery Evaluation Report,*. North Pacific Fishery Management Council.
674 Jurado-Molina, J., Livingston, P. A., & Ianelli, J. N. (2005). Incorporating predation interactions
675 in a statistical catch-at-age model for a predator-prey system in the eastern Bering Sea.
676 *Canadian Journal of Fisheries and Aquatic Sciences*, *62*(8), 1865–1873.
677 Kimmel, D., Axler, K., Cormack, B., Crouser, D., Fennie, W., Keister, J., Lamb, J., Pinger, C.,
678 Rogers, L., & Suryan, R. (2023). Current and Historical Trends for Zooplankton in the
679 Western Gulf of Alaska. In B. Ferris (Ed.), *Ecosystem Status Report 2023: Gulf of*
680 *Alaska, Stock Assessment and Fishery Evaluation Report*. North Pacific Fishery
681 Management Council.
682 Kingsolver, J., & Huey, R. (2008). Size, temperature, and fitness: Three rules. *Evolutionary*
683 *Ecology Research*, *10*(2), 251–268.
684 Kristensen, K. (2014). *TMB: General random effect model builder tool inspired by ADMB.*
685 https://github.com/kaskr/adcomp
686 Kristensen, K. (2024). *RTMB: "R" Bindings for "TMB."* https://CRAN.R-
687 project.org/package=RTMB
688 Lucey, S. M., Gaichas, S. K., & Aydin, K. Y. (2020). Conducting reproducible ecosystem
689 modeling using the open source mass balance model Rpath. *Ecological Modelling*, *427*,
690 109057. https://doi.org/10.1016/j.ecolmodel.2020.109057
691 Methot, R. D. (2009). Stock Assessment: Operational Models in Support of Fisheries
692 Management. In R. J. Beamish & B. J. Rothschild (Eds.), *The Future of Fisheries Science*
693 *in North America* (Vol. 31, pp. 137–165). Springer Netherlands.

694 Methot, R. D., & Taylor, I. G. (2011). Adjusting for bias due to variability of estimated
695 recruitments in fishery assessment models. *Canadian Journal of Fisheries and Aquatic*
696 *Sciences*, *68*(10), 1744–1760.
697 Monnahan, C. C., Adams, Grant D., Ferriss, B. E., Shotwell, S. Kalei, McKelvey, D.R., &
698 McGowan, David W. (2023). *Assessment of the walleye pollock stock in the Gulf of*
699 *Alaska* (Stock Assessment and Fishery Evaluation Report for Groundfish Resources of
700 the Gulf of Alaska). North Pacific Fishery Management Council. https://apps-
701 afsc.fisheries.noaa.gov/Plan_Team/2021/GOApollock.pdf
702 Monnahan, C. C., & Kristensen, K. (2018). No-U-turn sampling for fast Bayesian inference in
703 ADMB and TMB: Introducing the adnuts and tmbstan R packages. *PLOS ONE*, *13*(5),
704 e0197954. https://doi.org/10.1371/journal.pone.0197954
705 Morita, K., Fukuwaka, M., Tanimata, N., & Yamamura, O. (2010). Size-dependent thermal
706 preferences in a pelagic fish. *Oikos*, *119*(8), 1265–1272. https://doi.org/10.1111/j.1600-
707 0706.2009.18125.x
708 Neuenfeldt, S., Bartolino, V., Orio, A., Andersen, K. H., Andersen, N. G., Niiranen, S.,
709 Bergström, U., Ustups, D., Kulatska, N., & Casini, M. (2020). Feeding and growth of
710 Atlantic cod (Gadus morhua L.) in the eastern Baltic Sea under environmental change.
711 *ICES Journal of Marine Science*, *77*(2), 624–632. https://doi.org/10.1093/icesjms/fsz224
712 Oke, K. B., Cunningham, C. J., Westley, P. a. H., Baskett, M. L., Carlson, S. M., Clark, J.,
713 Hendry, A. P., Karatayev, V. A., Kendall, N. W., Kibele, J., Kindsvater, H. K.,
714 Kobayashi, K. M., Lewis, B., Munch, S., Reynolds, J. D., Vick, G. K., & Palkovacs, E. P.
715 (2020). Recent declines in salmon body size impact ecosystems and fisheries. *Nature*
716 *Communications*, *11*(1), 4155. https://doi.org/10.1038/s41467-020-17726-z

Oke, K. B., Mueter, F., & Litzow, M. A. (2022). Warming leads to opposite patterns in weight-at-age for young versus old age classes of Bering Sea walleye pollock. *Canadian Journal of Fisheries and Aquatic Sciences*, *79*(10), 1655–1666. https://doi.org/10.1139/cjfas-2021-0315

Polovina, J. J. (1984). Model of a coral reef ecosystem. *Coral Reefs*, *3*(1), 1–11. https://doi.org/10.1007/BF00306135

Scott, E., Serpetti, N., Steenbeek, J., & Heymans, J. J. (2016). A Stepwise Fitting Procedure for automated fitting of Ecopath with Ecosim models. *SoftwareX*, *5*, 25–30. https://doi.org/10.1016/j.softx.2016.02.002

Siple, M. C., von Szalay, P. G., Raring, N. W., Dowlin, A. N., & Riggle, B. C. (2024). *Data Report: 2023 Gulf of Alaska bottom trawl survey*. https://repository.library.noaa.gov/view/noaa/61491

Stock, B. C., Xu, H., Miller, T. J., Thorson, J. T., & Nye, J. A. (2021). Implementing two-dimensional autocorrelation in either survival or natural mortality improves a state-space assessment model for Southern New England-Mid Atlantic yellowtail flounder. *Fisheries Research*, *237*, 105873. https://doi.org/10.1016/j.fishres.2021.105873

Thorson, J. T., Arimitsu, M. L., Barnett, L. A. K., Cheng, W., Eisner, L. B., Haynie, A. C., Hermann, A. J., Holsman, K., Kimmel, D. G., Lomas, M. W., Richar, J., & Siddon, E. C. (2021). Forecasting community reassembly using climate-linked spatio-temporal ecosystem models. *Ecography*, *44*(4), 612–625. https://doi.org/10.1111/ecog.05471

Thorson, J. T., Johnson, K. F., Methot, R. D., & Taylor, I. G. (2017). Model-based estimates of effective sample size in stock assessment models using the Dirichlet-multinomial

distribution. *Fisheries Research*, *192*, 84–93. https://doi.org/10.1016/j.fishres.2016.06.005

Thorson, J. T., Kristensen, K., Aydin, K. Y., Gaichas, S. K., Kimmel, D. G., McHuron, E. A., Nielsen, J. M., Townsend, H., & Whitehouse, G. A. (2024). The benefits of hierarchical ecosystem models: Demonstration using EcoState, a new state-space mass-balance model. *Fish and Fisheries*. https://doi.org/10.1111/faf.12874

Thorson, J. T., Monnahan, C. C., & Cope, J. M. (2015). The potential impact of time-variation in vital rates on fisheries management targets for marine fishes. *Fisheries Research*, *169*, 8–17. https://doi.org/10.1016/j.fishres.2015.04.007

Thorson, J. T., Monnahan, C. C., & Hulson, P.-J. F. (2023). Data weighting: An iterative process linking surveys, data synthesis, and population models to evaluate mis-specification. *Fisheries Research*, *266*, 106762. https://doi.org/10.1016/j.fishres.2023.106762

Trathan, P. N., Warwick-Evans, V., Young, E. F., Friedlaender, A., Kim, J. H., & Kokubun, N. (2022). The ecosystem approach to management of the Antarctic krill fishery—The 'devils are in the detail' at small spatial and temporal scales. *Journal of Marine Systems*, *225*, 103598. https://doi.org/10.1016/j.jmarsys.2021.103598

Von Bertalanffy, L. (1960). Principles and theory of growth. *Fundamental Aspects of Normal and Malignant Growth*, *493*, 137–259.

Walters, C., Christensen, V., & Pauly, D. (1997). Structuring dynamic models of exploited ecosystems from trophic mass-balance assessments. *Reviews in Fish Biology and Fisheries*, *7*(2), 139–172. https://doi.org/10.1023/A:1018479526149

760 Walters, C., & Kitchell, J. F. (2001). Cultivation/depensation effects on juvenile survival and
761 recruitment: Implications for the theory of fishing. *Canadian Journal of Fisheries and*
762 *Aquatic Sciences*, *58*(1), 39–50.
763 Walters, C., Pauly, D., Christensen, V., & Kitchell, J. F. (2000). Representing Density
764 Dependent Consequences of Life History Strategies in Aquatic Ecosystems: EcoSim II.
765 *Ecosystems*, *3*(1), 70–83. https://doi.org/10.1007/s100210000011
766
767

Fig. 1 – Proportion at age (y-axis) for ages 1-31+ (x-axis) for sablefish in each year with available age-composition data (panels), showing measurements (colored histograms) and estimated value (red dots and lines), where estimates are the product of predicted abundance-at-age $v_{g2}(t)$ and selectivity-at-age. Bars are color-coded to have a single color for a given cohort across years, to facilitate comparison across years. Note that data are for ages 2-31+ (hence no bar for age-1), whereas the model predicts for ages 1-30+.

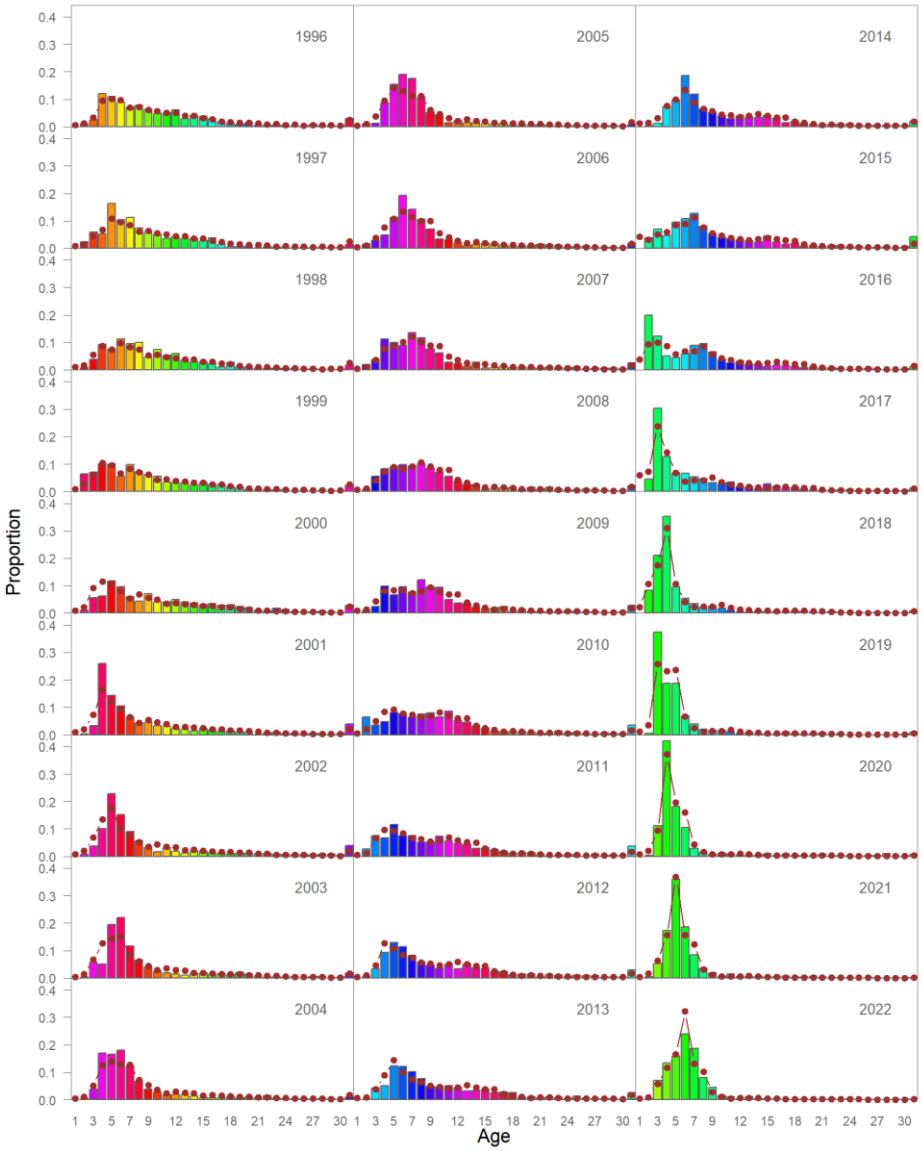

Fig. 2 – Estimated biomass (y-axis in million tons, with log-scale axis) in each year (x-axis) with available biomass-index data (1990-2023) and for the six functional groups that are affected by biomass indices (panels), showing observed values divided by the estimated catchability coefficient (dots) as well as the estimated value (black line) +/- 1.96 standard errors (shaded polygon)

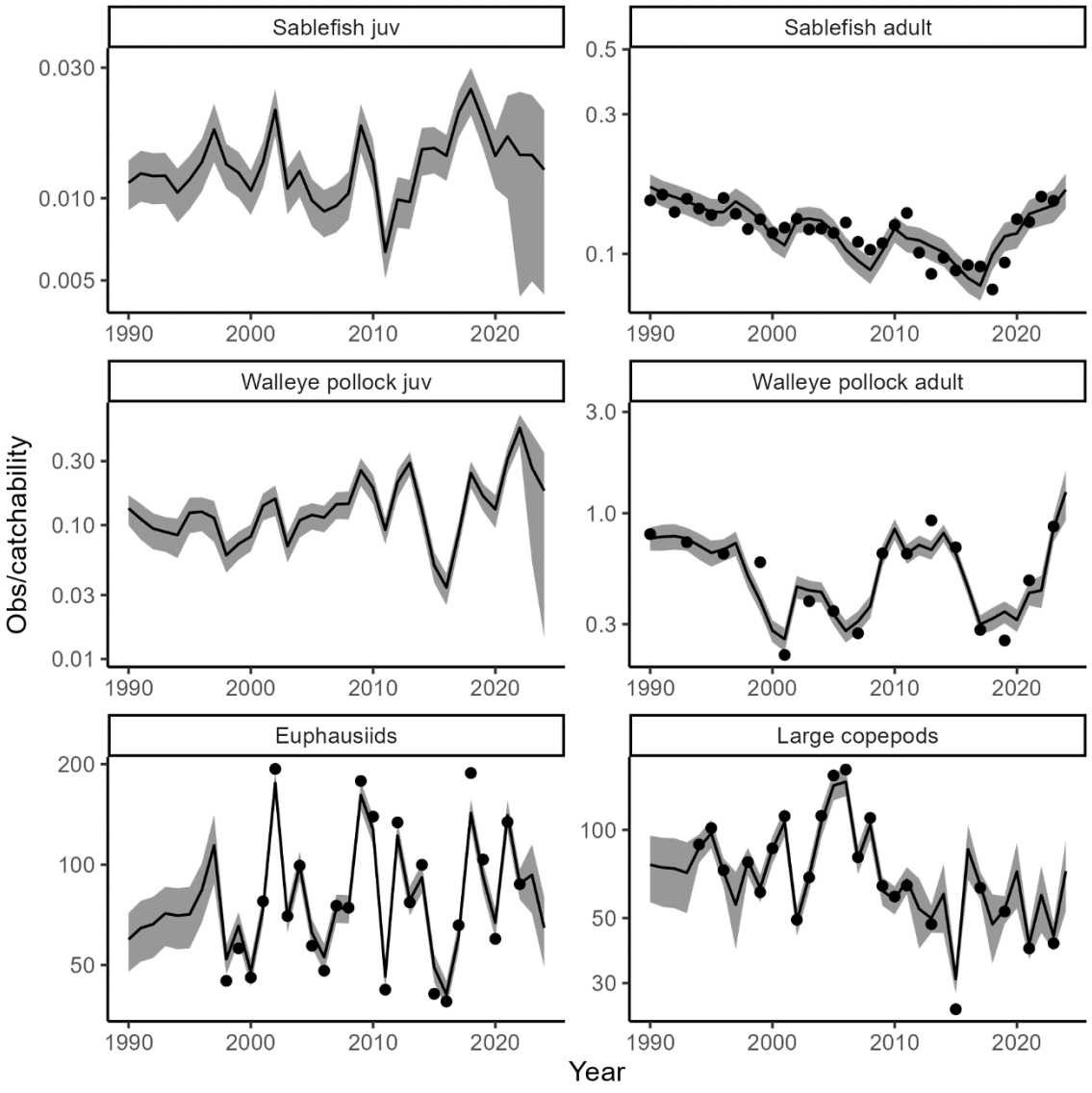

783 Fig. 3 – Proportion at age (y-axis) for ages 1-15+ (x-axis) for walleye pollock in each year with

784 available age-composition data (see Fig. 2 caption for details)

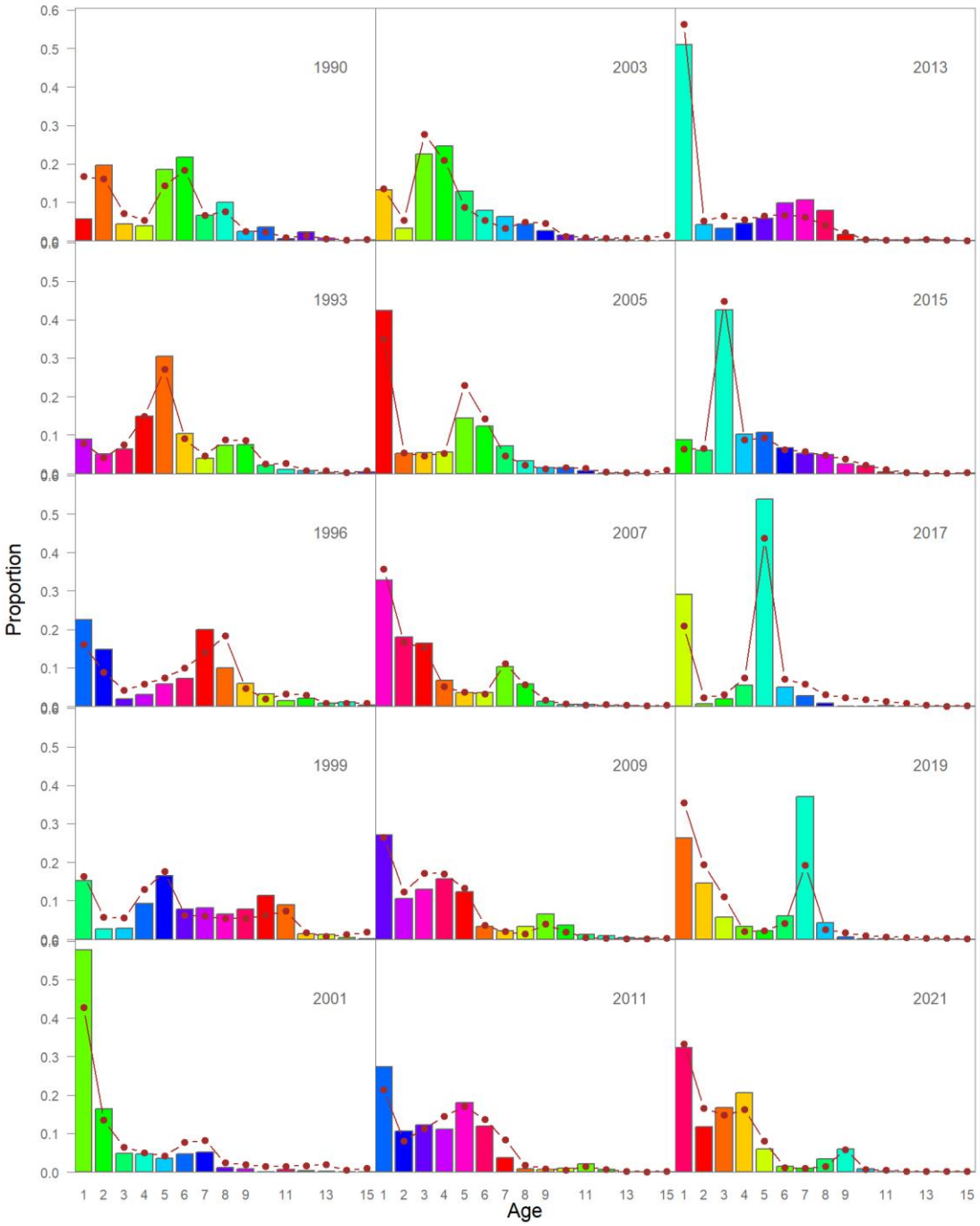

785

786

Fig. 4 – Estimated food web at equilibrium showing the proportion of pelagic production (x-axis) and the trophic level (y-axis) showing juvenile and adult sablefish (a and b), juvenile and adult pollock (d and e), and using alphabetical order for labelling taxa that are shown in Fig. S2.

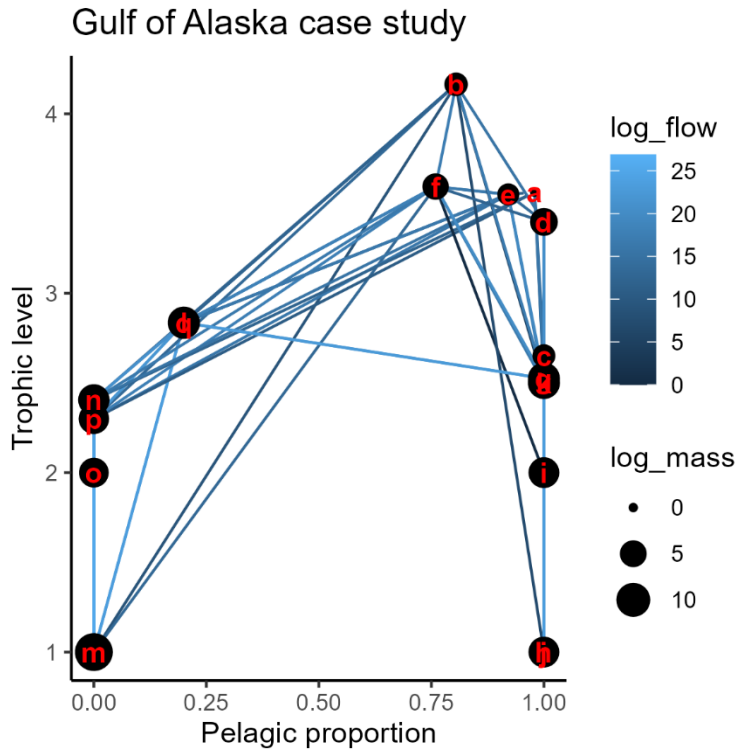

Fig. 5 – Comparison of predicted weight-at-age (top row) and withheld measurements that are not fitted (bottom row) for walleye pollock (left column) and sablefish (right column), showing the weight (y-axis) relative to equilibrium for the expected value or in KG for the observed value for each year with available data (x-axis). We compute the Spearman correlation over time for each age, and then the average correlation across ages for each species, and list that value in the top panels.

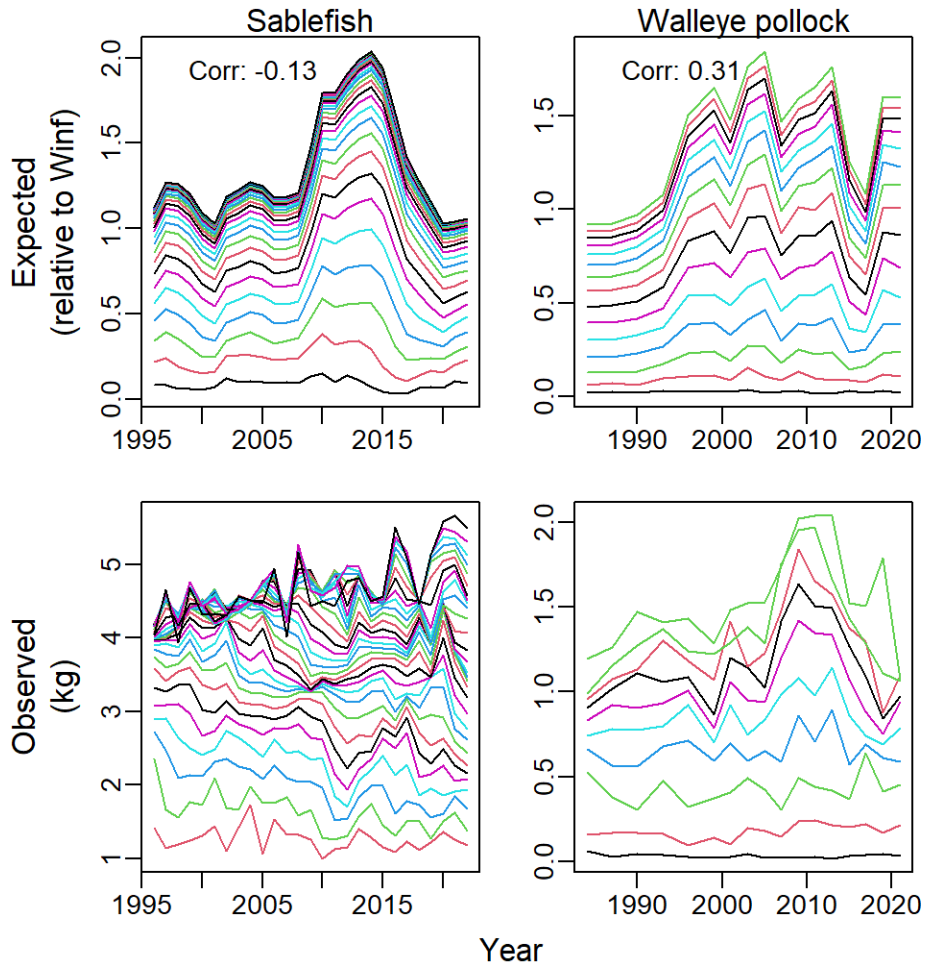

Fig. 6 – Retrospective peels for sablefish biomass (top row), pollock biomass (2nd row), sablefish recruitment deviation $\phi(t)$ (3rd row), or pollock recruitment deviation $\phi(t)$ (4th row) showing estimated values (y-axis) for 2011-2023 (x-axis) using data through 2023 (i.e., all data), 2022, 2021, …, or 2013, i.e. for ten retrospective peals (see colorbar on right-hand side), showing the dot (line) and 95% confidence interval (+/- 1.96 standard errors, whiskers) for each run.

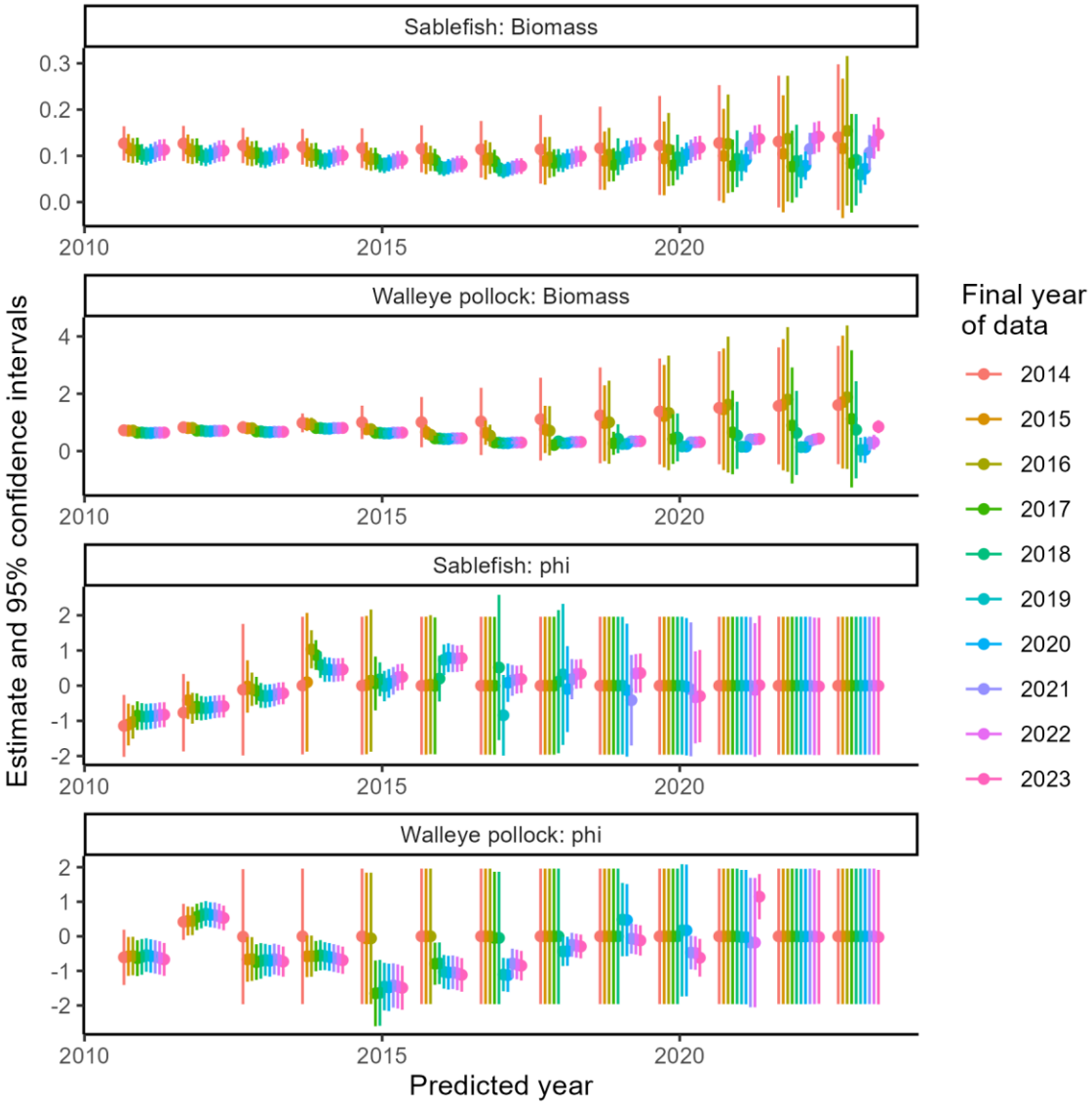

Table 1 – Equations from Ecostate prior to incorporating age-structured dynamics (i.e., summarizing Thorson et al., 2024). Note that Eq. T1.1 is replaced when estimating annual variation in consumption.

Eq.	Description	Equation
T1.1	Consumption rate	$c_{i,j}(t) = \underbrace{\bar{c}_{i,j}}_{\text{equilibrium consumption rate}} \times \underbrace{\frac{x_{i,j}\frac{\beta_j(t)}{\bar{\beta}_j}}{x_{i,j} - 1 + \frac{\beta_j(t)}{\bar{\beta}_j}}}_{\text{predator functional response}} \times \underbrace{\frac{\frac{\beta_i(t)}{\bar{\beta}_i}}{}}_{\text{prey functional response}}$
T1.2	Population mortality rate	$m_s(t) = \underbrace{\frac{\sum_{j=1}^{S} c_{s,j}(t)}{\beta_s(t)}}_{\text{Predation rate}} + \begin{cases} \underbrace{p_s(1-e_s)}_{\text{Residual natural mortality rate}} & \text{if } s \text{ is autotroph or heterotroph} \\ \underbrace{v_s}_{\text{Export rate}} & \text{if } s \text{ is detritus} \end{cases}$
T1.3	Detritus turnover rate	$\bar{\beta}_s v_s = \underbrace{\sum_{i=1}^{S}\sum_{j=1}^{S} u_j \bar{c}_{i,j}(t) + \sum_{j=1}^{S} \bar{\beta}_j p_s (1-e_s)}_{\text{Detritus accumulation}} - \underbrace{\sum_{j=1}^{S} \bar{c}_{s,j}(t)}_{\text{Detritus consumption}}$
T1.4	Population growth rate	$g_s(t) = \begin{cases} \frac{p_s}{w_s} \times \frac{\sum_{i=1}^{S} c_{i,s}(t)}{\beta_s(t)} & \text{if } s \text{ is heterotroph} \\ \frac{p_s \bar{\beta}_s}{\beta_s(t)} \times \frac{x_{s,s}\frac{\beta_s(t)}{\bar{\beta}_s}}{x_{s,s} - 1 + \frac{\beta_s(t)}{\bar{\beta}_s}} & \text{if } s \text{ is autotroph} \\ \frac{\sum_{i=1}^{S}\sum_{j=1}^{S} u_j c_{i,j}(t) + \sum_{j=1}^{S} \beta_j(t) p_j (1-e_j)}{\beta_s(t)} & \text{if } s \text{ is detritus} \end{cases}$
T1.5	Measurement error for biomass index	$\log(b_s(t)) \sim \text{Normal}(\log(q_s \beta_s(t)), \sigma_s^2)$

T1.6	Measurement error for fishery catch	$\log(h_s(t)) \sim \text{Normal}(\log(\eta_s(t)), \nu_s^2)$
T1.7	Process error for biomass rates	$\epsilon_s(t) \sim \text{Normal}(0, \tau_s^2)$

809

Table 2 – List of estimated parameters for the two age-structured populations (sablefish and walleye pollock) in the Gulf of Alaska case study, where juveniles are ages [0-2) and adults are ages [2,15+] for pollock and [2,31+] for sablefish, where equilibrium values refer to unfished equilibrium. For estimated parameters, we show the estimate with standard error in parentheses (note that the standard error for predicted trophic level is small because forage species have biomass that is fixed at Rpath values). For values fixed *a priori*, we show the fixed value without standard error. At age 50% maturity for walleye pollock is calculated as an average from 1983-2023 based on annual regression estimates (see Fig 1.18 of Monnahan et al. (2023) for original data). Uncertainty about equilibrium biomass is not typically calculated for age-structured stock assessments and not included here. Pollock age-maturity from the stock assessment is calculated as the average of an annual value; pther values for assessment are listed as "-" when not available.

	Ecostate estimate (standard error)		Stock assessments	
Parameter	Sablefish	Pollock	Sablefish	Pollock
Equilibrium juvenile biomass (million tons)	0.014 (0.003)	0.192 (0.059)	-	0.252
Equilibrium adult biomass (million tons)	0.361 (0.049)	1.609 (0.415)	0.716	2.333
Equilibrium juvenile natural mortality rate (yr^{-1})	1.65	1.96	-	1.39
Equilibrium adult natural mortality rate (yr^{-1})	0.095 (0.029)	0.408 (0.106)	0.114	0.3
Equilibrium juvenile trophic level (unitless)	3.563 (<0.001)	3.55 (<0.001)	-	-
Equilibrium adult trophic level (unitless)	4.164 (<0.001)	3.594 (<0.001)	-	-
Steepness (unitless)	0.999	0.999	1	1
Equilibrium age at maturity (yr)	6	4	7	4.742
Equilibrium von Bertalanffy growth (yr^{-1})	0.14	0.2	0.202	-
Allometric consumption by weight (unitless)	0.5	0.667	-	-
Catchability coefficient (unitless)	10.191 (3.226)	1.025 (0.312)	6.359	0.800
Age at 50% survey selectivity (yr)	3.917 (0.09)	5.944 (0.42)	3.004	4.00
Slope for logistic survey selectivity (yr^{-1})	0.559 (0.042)	1.365 (0.08)	2.418	0.637
Vulnerability $x_{ij} = x_j$ for predator j (unitless)	1.595 (0.362)	3.259 (1.334)	-	-

Supplementary Materials 1: Additional figures

Table S1 – Notation used in the model presentation and results, including the symbol, units, a brief description, and the type. See Thorson et al. (2024) Table S1 for notation related to biomass dynamics.

Symbol	Units	Description	Type
a^*	-	Fractional age, discretized within integer age a	Index
t^*	-	Fractional time, discretized within integer time t	Index
s	-	Functional group	Index
$s2$	-	Stanza within an age-structured population	Index
$g2$	-	Age-structured population	Index
$n_{a,t}$	$numbers$	Age-composition samples for integer age and year	Data
$w_{a,t}$	$mass/number$	Empirical weight-at-age data for integer age and year	Data
b	$unitless$	Allometric scaling of individual mass to length	Specified
n_Δ	$number$	Number of fractional per integer time	Specified
ω_{a^*,t^*}	$mass/number$	Average weight for fractional age a^* and fractional time t^*	Estimated
$\omega_{a,t}$	$mass/number$	Average weight for integer age a and time integer time t	Estimated
v_{a^*,t^*}	$numbers$	Abundance for fractional age a^* and fractional time t^*	Estimated
$v_{a,t}$	$numbers$	Abundance for integer age a and time integer time t	Estimated
k	$time^{-1}$	Specialized Von Bertalanffy growth rate for length	Estimated
d	$unitless$	Allometric scaling of consumption to animal mass	Estimated
(θ_1, θ_2)	$unitless$	Logistic selectivity-at-age parameters	Estimated
θ_3	$unitless$	Optional logit-ratio of effective to input sample size	Estimated
σ_w^2	$unitless$	Residual variance in weight-at-age data	Estimated
$\phi_{g2}(t)$	$unitless$	Recruitment deviations	Estimated
σ_ϕ^2	$unitless$	Variance of recruitment deviations	Estimated
$\nu_j(t)$	$unitless$	Consumption deviations	Estimated
$\sigma_{\nu,j}^2$	$unitless$	Variance of consumption deviations	Estimated
H	$mass/mass^d$	Anabolic rate	Derived
K	$time^{-1}$	Generalized von Bertalanffy growth rate for mass	Derived
L_∞	$length$	Asymptotic maximum body length	Derived
$\beta_{s,t}$	$mass$	Estimated biomass for functional group s in time t	Derived
ω_∞	$mass/number$	Asymptotic maximum body mass	
$\bar{\omega}_a$	$mass/number$	Equilibrium weight-at-integer age	Derived

$\bar{v}_a$	$numbers$	Equilibrium abundance-at-integer-age	Derived
$\bar{\beta}_s$	$mass$	Equilibrium unfished biomass for functional group s	Derived
$\bar{\omega}_{a^*}$	$mass /number$	Equilibrium weight-at-fractional age	Derived
$\bar{v}_{a^*}$	$numbers$	Equilibrium abundance-at- fractional -age	Derived
$\bar{\alpha}_{a^*}$	$unitless$	Convert consumption per biomass for a stanza to individual growth per fractional age	Derived
$g_{s,t}$			

824

825

826

Fig. S1 – Comparison of biomass (left column with log-scale y-axis) over 70 years (x-axis) for two stanzas of walleye pollock (juv: ages [0-2) year; adult: ages [2,11+]), abundance-at-age (middle column with log-scale y-axis), and weight-at-age (right column with natural-scale y-axis) when (1) projecting without catch to demonstrate that the model stays in equilibrium (top row), and (2) when projecting as fishing mortality increases from 0 to 0.2 yr^{-1} to demonstrate the density-dependent increase in weight-at-age (bottom right) and recruitment (bottom-left) as abundance-at-age decreases (bottom middle) over time.

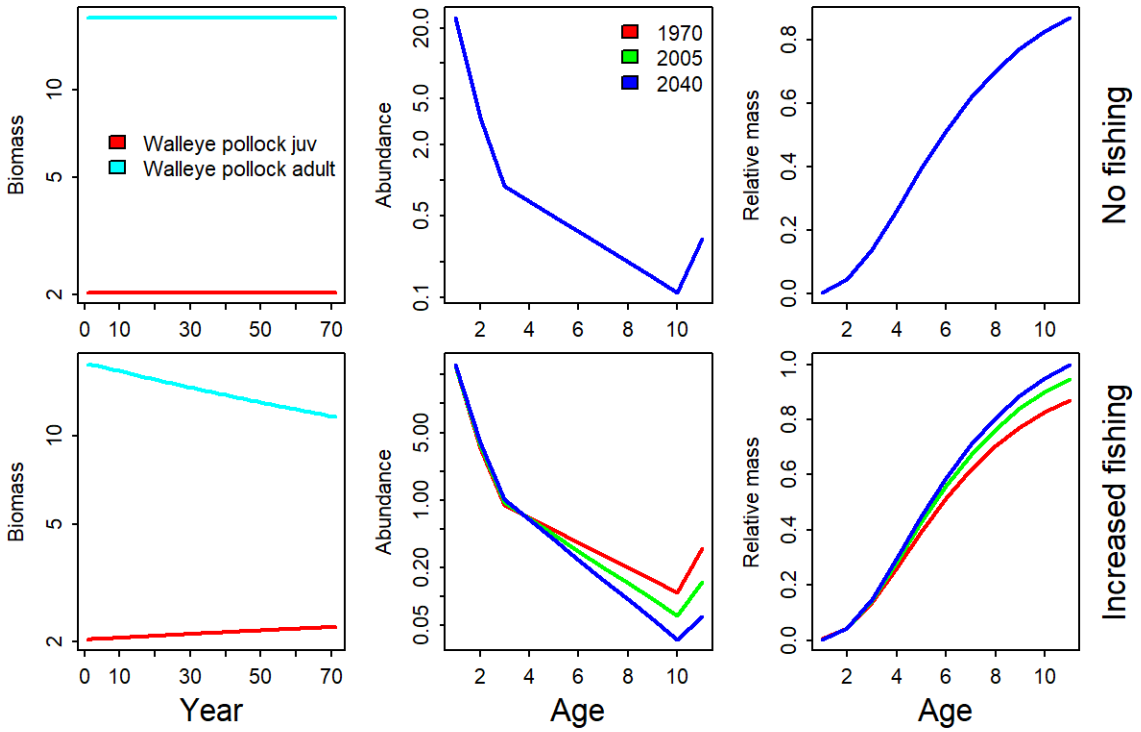

Fig. S2 – Estimated biomass relative to average unfished equilibrium (y-axis) in each modeled year (x-axis, 1960-2040), showing the estimated value (black line) +/- 1.96 standard errors (shaded polygon), and indicating the forecast period with a dotted vertical line at 2023.5

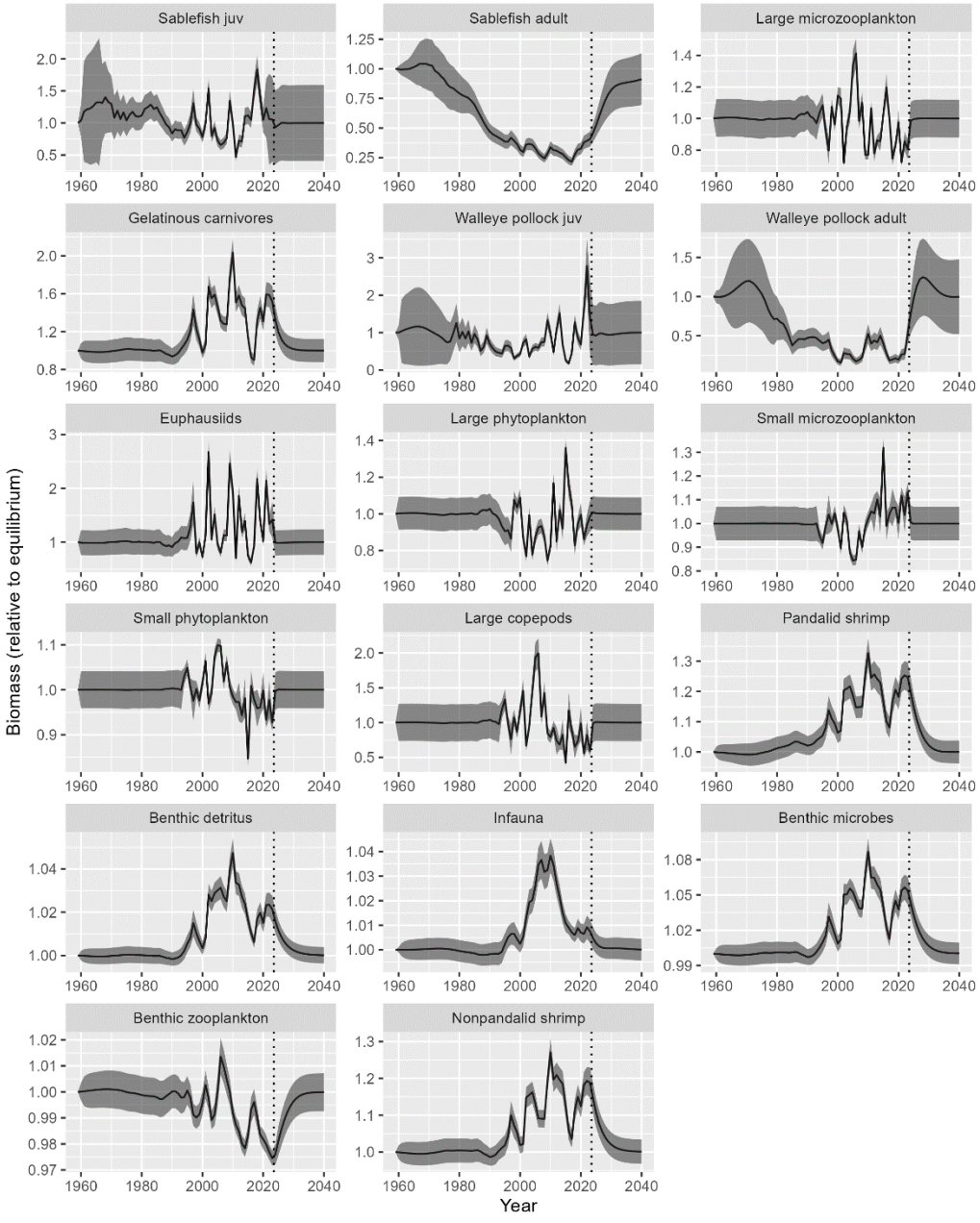

Fig. S3 – Estimated weight relative to asymptotic maximum (y-axis) in each year (x-axis) for each modeled age (colored lines, top row on log-scale), consumption relative to equilibrium (2nd row on log-scale) for juveniles (red line) and adults (blue line), as well as juvenile (3rd row) and adult (bottom row) diet proportions relative to equilibrium (with code legend in panels) for sablefish (left column) and walleye pollock (right column), where the diet proportions (3rd and 4th rows) have total that matches relative consumption (2nd row). In the first row, we show weight relative to asymptotic maximum weight (ω_∞), and in other rows we show consumption relative the equilibrium unfished level of consumption, with a horizontal dashed line at the equilibrium of 1.0.

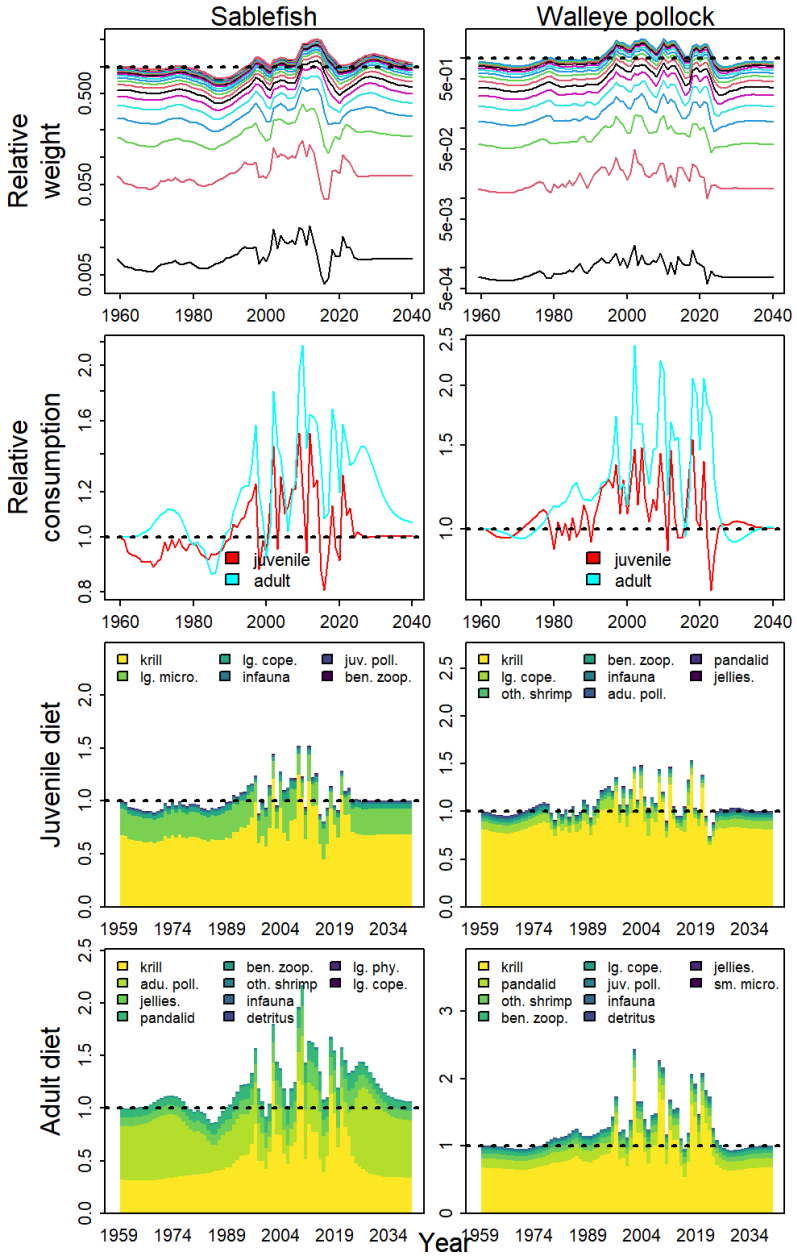

Fig. S4 – Comparison of expected weight-at-age (top row), observed weight-at-age (middle row), and smoothed weight-at-age including year, age, and cohort effects for walleye pollock (left column) and sablefish (right column). See Fig. 5 caption for more details.

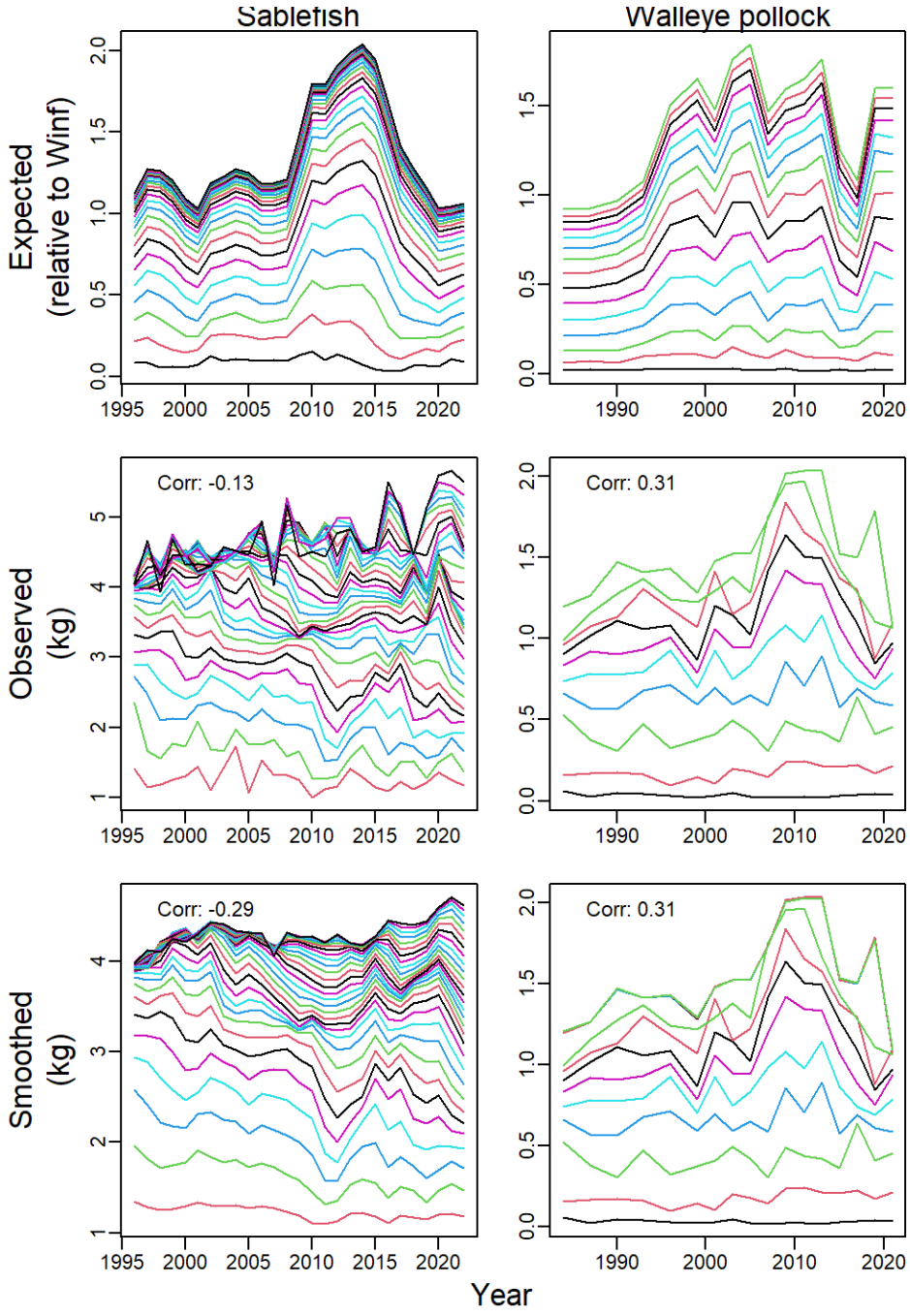

Fig. S5 – Estimated biomass (y-axis in million tons, with log-scale axis) in each year (x-axis) with available biomass-index data (1990-2023) and for the six functional groups (see Fig. 2 caption for details) when removing indices for copepods and euphausiids

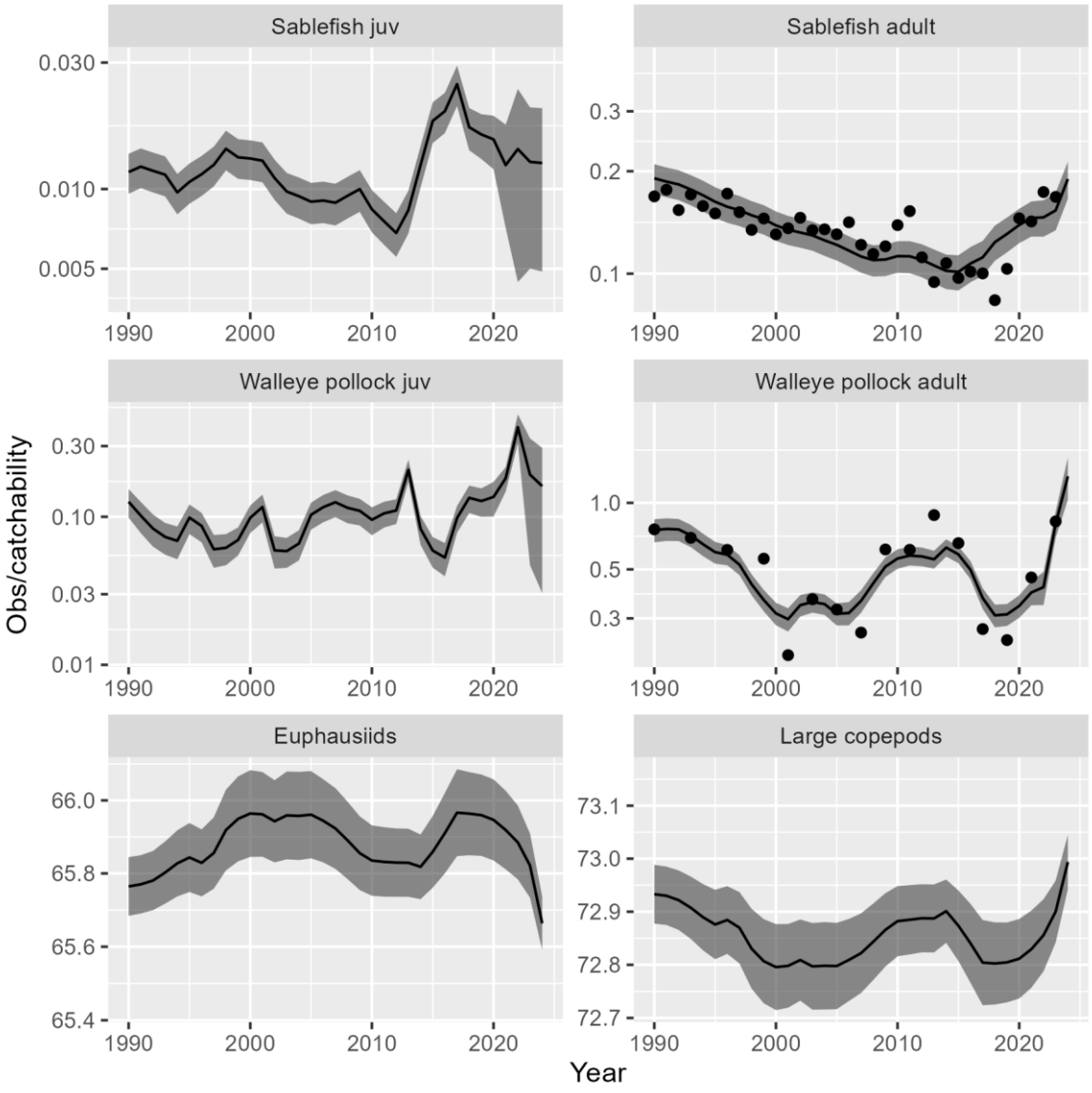

Fig. S6 -- Comparison of expected weight-at-age (top row) and observed weight-at-age (bottom row) for walleye pollock (left column) and sablefish (see Fig. 5 caption for details), in a model identical to the base case but without fitting to biomass indices for euphausiids and large copepods.

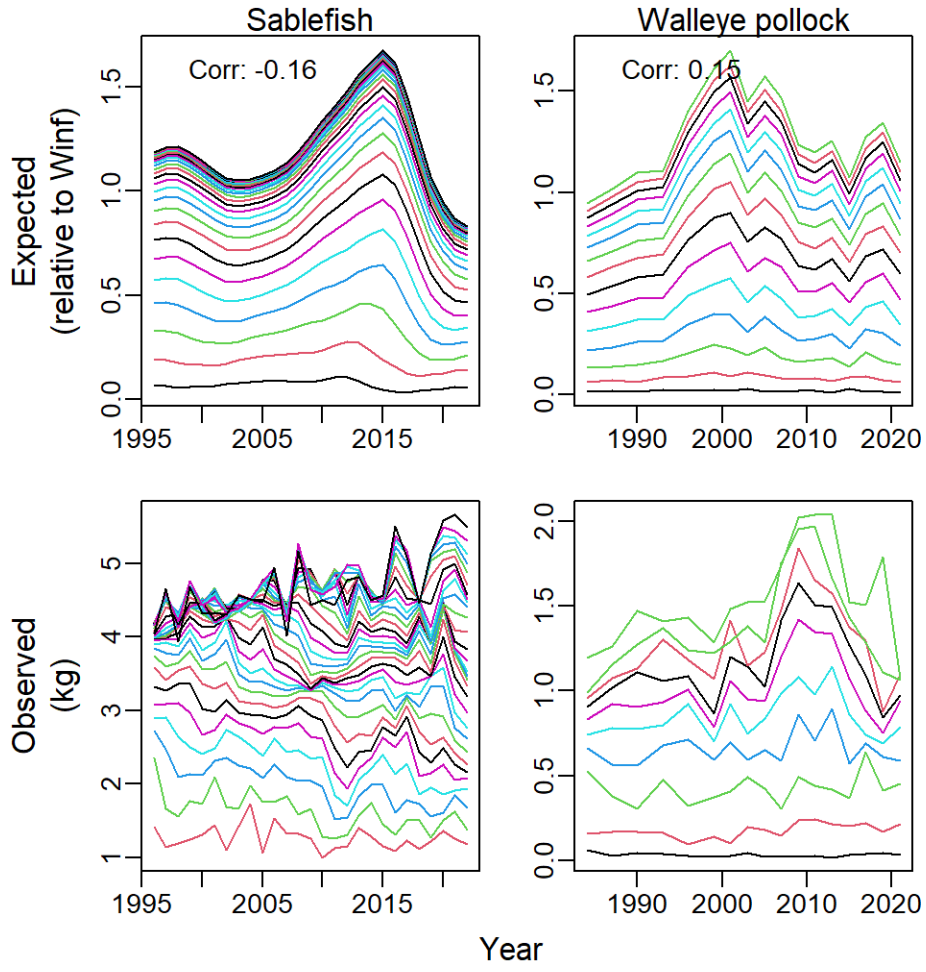

Supplementary Materials 2: Detailed notation for an age-structured model with bottom-up and top-down control

Having introduce the theory that connects population to individual mortality and growth rates, we now discuss the model implementation in detail. Each age-structured population requires specifying or estimating the von Bertalanffy growth rate k, weight-at-maturity w_{mat} and stock-recruit parameter x_{spawn} and each stanza-group $s2$ has a maximum-age $a_{\mathrm{max},s2}$ such that it represents a range of ages $a_{\mathrm{min},s2} \leq a < a_{\mathrm{max},s2}$, where $a_{\mathrm{min},s2} = 0$ for the stanza-group with the youngest maximum age, or otherwise $a_{\mathrm{min},s2} = a_{\mathrm{max},s2-1}$ where $s2 - 1$ is the stanza-group with the next-youngest maximum age. Diet proportions are specified for each functional group s, such that all ages in a given stanza-group are assumed to have the same diet. It is therefore customary to break an age-structured population into multiple stanzas at ages that correspond to shifts in diet. However, we note that it is possible to specify an age-structured population with a single stanza-group, and proceed with fitting age-composition and/or weight-at-age data for that single stanza. In this case, the age-composition data might be informative about natural mortality rates and/or the catchability coefficient.

Specifying dynamics for an age-structured population requires tracking abundance-at-age $\nu_a(t)$ and weight-at-age $\omega_a(t)$ (using Greek letters for "n" and "w" for abundance and weight). Biomass $\boldsymbol{\beta}(t)$ is still integrated for every $t \in \{1,2,\ldots,T\}$ (applying an ODE solver to using Eq. 2), but we also integrate abundance-at-age and weight-at-age in parallel using a separate Euler approximation with n_Δ sub-intervals. After projecting abundance for n_Δ sub-intervals, we then increase the calendar age of all fishes, calculate the total biomass for each stanza-group after increasing ages, and replace $\boldsymbol{\beta}(t)$ from integrating Eq. 2 with biomass from integrating age-

structured dynamics (where these two will closely match prior to increasing calendar age for each fish).

To implement the Euler approximation for age-structured dynamics using $\Delta \in \{1,2,\ldots,n_\Delta\}$ sub-intervals, we therefore track abundance-at-age $v^*_{a^*,g2}(t^*)$ and weight-at-age $\omega^*_{a^*,g2}(t^*)$ using fractional age $a^* = n_\Delta a + \Delta$ and fractional time $t^* = n_\Delta t + \Delta$, where calendar age $a = \frac{a^*}{n_\Delta}$ and calendar year $t = \frac{t^*}{n_\Delta}$, and where biomass for a given stanza-group $s2$ matches $\beta_{s[s2]}$ at each integer calendar year t:

$$\beta_{s[s2]}(t) = \sum_{a^*=n_\Delta a_{\min,s2}}^{n_\Delta a_{\max,s2}} v^*_{a^*,g2}(t)\omega^*_{a^*,g2}(t) \tag{3}$$

We first calculate equilibrium abundance-at-age $\bar{v}^*{}_{a^*,g2}$, equilibrium weight-at-age $\bar{\omega}^*{}_{a^*,g2}$, and consumptive demand $\alpha_{a^*,g2}$. As overview for doing so, we start with the value for production-per-biomass $p_{s[s2]}$ for all stanza-groups $s2$, and both equilibrium biomass $\bar{\beta}_{s[s2]}$ and consumption per biomass $w_{s[s2]}$ for a single "leading" stanza. These values can either be fixed a priori, or subsequently estimated by maximizing the log-likelihood of available data. Equilibrium biomass and consumption per biomass for non-leading stanzas are then calculated from values for the leading stanza, such that equilibrium consumption and biomass (Eq. 1) are satisfied.

In particular, we specify that equilibrium weight-at-age follows a generalized von Bertalanffy growth function (and defined relative to asymptotic maximum weight for computational efficiency), noting that fractional calendar age during subinterval Δ is $\frac{a^*}{n_\Delta}$:

$$\bar{\omega}^*{}_{a^*,g2} = \left(1 - e^{-3k_{g2}(1-d)\frac{a^*}{n_\Delta}}\right)^{\frac{1}{1-d}} \tag{4}$$

Similarly, we specify the stable age-distribution:

$$\bar{v}^*_{a^*,g2} = \begin{cases} \bar{R}_{g2} & \text{if } a^* = 0 \\ \bar{v}^*_{a^*-1,g2} e^{-\frac{Z_{s2}}{n_\Delta}} & \text{if } 0 < a^* < n_\Delta a_{\max,g2} \\ \bar{v}^*_{a^*-1,g2} \dfrac{e^{-\frac{Z_{s2}}{n_\Delta}}}{1 - e^{-\frac{Z_{s2}}{n_\Delta}}} & \text{if } a^* = n_\Delta a_{\max,g2} \end{cases} \quad (5)$$

Where mortality rate $Z_{s2} = p_{s2}$ is equal to production per biomass rate at equilibrium for each stanza, and we treat the maximum fractional age $n_\Delta a_{\max,g2}$ for the oldest stanza-group as a plus-group. We then calculate the proportion mature at age, which is used to calculate spawning biomass. For consistency with EwE, the user can specify the weight $\omega_{\text{mat},g2}$ of a knife-edged maturation ogive, where fecundity is $\omega - \omega_{\text{mat},g2}$ for weight ω above $\omega_{\text{mat},g2}$ and zero otherwise. Alternatively, we allow the user to specify either:

1. Age at maturity $a_{\text{mat},g2}$, where the model solves for weight-at-maturity $\omega_{\text{mat},g2}$ given the values for d and k; and/or
2. Logistic maturity at age with logistic slope $\omega_{\text{matslope},g2}$ (representing a logistic maturity ogive) where fecundity is $\omega\left(1 + e^{-\omega_{\text{matslope},g2}(\omega - \omega_{\text{mat},g2})}\right)^{-1}$;

Model exploration suggests that a logistic maturity ogive is more numerically stable, i.e., avoids $\beta_s(t)$ for recruits in years when consumption is low and all age-classes have body size lower than $\omega_{\text{mat},g2}$.

Given this equilibrium abundance, weight, and maturity-at-age, we then calculate equilibrium spawning biomass per recruit, use this to solve for the equilibrium recruitment $\bar{R}_{g2}$ per interval Δ that results in $\beta_{s[s2]} = \bar{\beta}_{s[s2]}$ for the leading stanza, and then use $\bar{R}_{g2}$ and the equilibrium survival-at-age and weight-at-age to calculate equilibrium biomass $\bar{\beta}_{s[s2]}$ for the

924 other (nonleading) stanzas. Finally, we calculate equilibrium spawning biomass, where this and
925 $\bar{R}_{g2}$ contribute to the stock-recruit relationship.

926 Given these equilibrium calculations, we project abundance-at-age and weight-at-age
927 using the Euler approximation involving fractional ages and time. Specifically, abundance-at-
928 age decreases based on instantaneous natural and fishing mortality rates:

$$\nu^*_{a^*+1,g2}(t^*+1) \tag{6A}$$

$$= \begin{cases} e^{\frac{-m_{s[s2]}(t^*)-f_{s[s2]}(t^*)}{n_\Delta}} \nu^*_{a^*,g2}(t^*) & \text{if a} + 1 < n_\Delta a_{\max,g2} \\ e^{\frac{-m_{s[s2]}(t^*)-f_{s[s2]}(t^*)}{n_\Delta}} \left(\nu^*_{a^*,g2}(t^*) + \nu^*_{a^*+1,g2}(t^*)\right) & \text{otherwise} \end{cases}$$

929 Where $m_{s[s2]}(t^*)$ is the population mortality rate from the ODE solver for biomass dynamics
930 (i.e., when numerically solving Eq. 2). Similarly, weight-at-age changes based on estimated
931 growth increments (Eq. 4-5), where consumption Q_s is again extracted from the numerical
932 solution for the biomass ODE. These projections result in a decrease in average age and
933 (typically) an increase in weight-at-age as fishing mortality increases for a targeted species (Fig.
934 S1), where the latter arises due to the predicted increase in per-capita consumption.

935 Following Ecosim, we assume that recruitment occurs continuously, i.e., evenly in each
936 fractional time Δ. To model recruitment, we first calculate mature biomass $\beta_{\text{mat}}(t^*)$:

937 $$\beta_{\text{mat}}(t^*) = \sum_{a=0}^{a_{\max,g2}} \nu^*_{a^*}(t^*) \times f\left(\omega^*_{a^*}(t^*), \omega_{\text{mat}}, \omega_{\text{matslope}}\right)$$

938 Where $f\left(\omega, \omega_{\text{mat}}, \omega_{\text{matslope}}\right)$ is the maturity ogive. We then calculate recruitment from mature
939 biomass relative to its equilibrium level $\frac{\beta_{\text{mat}}(t^*)}{\bar{\beta}_{\text{mat}}}$:

$$v_1^*(t^*) = \bar{R}_{g2} \times \underbrace{\frac{x_{\text{spawn}}}{x_{\text{spawn}} - 1 + \frac{\beta_{\text{mat}}(t^*)}{\bar{\beta}_{\text{mat}}}}}_{\substack{\text{Beverton–Holt} \\ \text{relationship}}} \times \underbrace{e^{\phi(t)}}_{\substack{\text{recruitment} \\ \text{deviation}}}$$

Where x_{spawn} is the magnitude of compensatory recruitment, which can be calculated from the proportion of equilibrium recruitment expected at 20% of equilibrium spawning biomass (termed "steepness" h) using the expression $h = \frac{0.2x_{\text{spawn}}}{x_{\text{spawn}} - 1 + 0.2}$ or equivalently $x_{\text{spawn}} = \frac{4}{5 - h^{-1}}$. Similarly, $\phi(t)$ represents otherwise unexplained variation in cohort strength (a "recruitment deviation").

After projecting fractional abundance $v^*_{a^*,g2}(t^*)$ and weight-at-age $\omega^*_{a,g2}(t^*)$ for n_Δ steps (i.e., a full integer time t), we then calculate average abundance and weight for integer ages:

$$v_{a,g2}(t+1) = \frac{1}{n_\Delta} \sum_{a^* = n_\Delta a}^{n_\Delta(a+1)-1} v^*_{a^*,g2}\big(n_\Delta(t+1)\big)$$

$$\omega_{a,g2}(t+1) = \frac{1}{n_\Delta} \sum_{a^* = n_\Delta a}^{n_\Delta(a+1)-1} \omega^*_{a^*,g2}\big(n_\Delta(t+1)\big)$$

We can then compare these predictions with observations, as a component of a model likelihood.